Indian J Phys
https://doi.org/10.1007/s12648-025-03883-8

ORIGINAL PAPER

Theoretical investigations on structural, electronic, mechanical, optical, dynamic, thermal, and hydrogen storage properties of $MGaH_4$ (M = Li, Na, K, Rb, Cs)

C Kürkçü[1]* and Ç Yamçıçıer[2]

[1]Department of Electronics and Automation, Kırşehir Ahi Evran University, Kırşehir, Turkey

[2]Department of Electricity and Energy, Osmaniye Korkut Ata University, Osmaniye, Turkey

Received: 25 June 2025 / Accepted: 19 November 2025

Abstract: This study presents a comprehensive first-principles investigation of the structural, electronic, mechanical, optical, dynamical, thermal, and hydrogen storage properties of $MGaH_4$ (M = Li, Na, K, Rb, Cs) hydrides using density functional theory. The optimized crystal structures reveal that $LiGaH_4$ and $NaGaH_4$ crystallize in the Cmcm space group, while $KGaH_4$, $RbGaH_4$, and $CsGaH_4$ crystallize in the Pnma space group. All compounds exhibit thermodynamic stability with negative formation enthalpies ranging from − 0.154 eV/atom ($LiGaH_4$) to − 0.248 eV/atom ($CsGaH_4$). Cohesive energies vary between 3.110 and 3.173 eV/atom, confirming strong internal bonding. Mechanical analysis demonstrates mechanical stability for all compounds, with elastic constants satisfying Born–Huang criteria. The polycrystalline bulk moduli (8.26–16.33 GPa), shear moduli (5.47–11.46 GPa), and Young's moduli (13.44–27.54 GPa) indicate relatively soft and brittle behavior (B/G < 1.75). Hardness calculations yield average Vickers hardness values of 0.88–2.87 GPa, confirming their soft nature. Phonon dispersion spectra show no imaginary frequencies, confirming dynamical stability. Electronic band structures reveal wide band gaps, confirming semiconducting behavior: 4.57 eV ($LiGaH_4$), 4.68 eV ($NaGaH_4$), 5.00 eV ($KGaH_4$), 5.00 eV ($RbGaH_4$), and 4.93 eV ($CsGaH_4$). Optical analysis demonstrates high ultraviolet absorption (maximum absorption coefficient up to 13.1 × 10^5 cm^{-1} for $CsGaH_4$), high reflectivity in the UV region (maximum 36% for $NaGaH_4$), and optical transparency in the visible range. Thermal properties reveal Debye temperatures between 168.26 K ($CsGaH_4$) and 352.04 K ($LiGaH_4$), while melting temperatures range from 428.38 to 553.64 K. Minimum thermal conductivities are found between 0.29 and 0.72 W/m·K. Hydrogen storage analysis shows that $LiGaH_4$ possesses the highest gravimetric (5.00 wt%) and volumetric (92.81 gH_2L^{-1}) storage capacities, approaching the U.S. DOE 2025 gravimetric target (5.5 wt%) and exceeding the volumetric target (40 gH_2L^{-1}). The desorption temperatures range from 113.70 K ($LiGaH_4$) to 183.01 K ($CsGaH_4$), suggesting relatively low hydrogen release energy barriers. Among the studied compounds, $LiGaH_4$ demonstrates superior performance owing to its high storage capacity, strong bonding (Ecoh = 3.173 eV/atom), high Debye temperature (352.04 K), and wide band gap (4.57 eV). Overall, the results highlight $LiGaH_4$ as the most promising candidate for lightweight solid-state hydrogen storage, while providing systematic insights into the role of alkali cation size on the stability, mechanical robustness, electronic band gap, optical absorption, and storage performance of $MGaH_4$ hydrides.

Keywords: Hydrogen storage; Structural; Electronic; Elastic; Optic; Phonon

1. Introduction

Energy demand is consistently rising as a result of variables such as improving living standards and population expansion. The International Energy Agency (IEA) reports that the predominant source of meeting this demand is now fossil fuels [1, 2]. Regrettably, the extensive dependence on fossil fuels has resulted in human-caused carbon dioxide (CO_2) emissions, hence exacerbating the occurrence of extreme climate phenomena, including droughts, floods, and deforestation. Researchers caution that a 2 degrees Celsius increase in the average global temperature presents a substantial hazard to the survival of life on our planet.

*Corresponding author, E-mail: ckurkcu@ahievran.edu.tr

Published online: 05 December 2025

Green hydrogen has the potential to reduce carbon emissions in high-demand industrial sectors like steel and cement. The world's demand for hydrogen is expected to rise by 700% by 2050, compared to the 70 million tons of hydrogen that are produced each year now [3, 4]. Some countries, like Chile, Norway, and the United States of America (USA), have put in place industrial policies that have helped them become world leaders in their areas. These proactive steps can speed up the general use of green hydrogen and lead to new developments in the business world. Because of these worries, a lot of work has gone into finding clean, long-lasting, useful, and good world energy sources and other ways to transport energy [5, 6].

The pressing need for sustainable energy sources is made clear by the fact that oil reserves are running out and energy needs are rising. These resources are running out at a worrisome rate because fossil fuels are being used up so quickly. The main way that hydrogen from fossil fuels is used is in industry, which is expected to affect green hydrogen value chains [4, 7]. Hydrogen is better than fossil fuels because it has fewer bad effects on the environment. Hydrogen is not physically kept in the structure of the metal; instead, it is stored in the solid as an oxide. This makes it easy to turn hydrogen into steam and then back into hydrogen by reducing steam [8].

Hydrogen is a clean form of energy that doesn't harm the world when it's burned [9, 10]. Researchers are interested in hydrogen as a possible material for making fuel in the future because it has unique qualities [9]. Besides that, hydrogen has the most energy per unit mass [11, 12]. So, it can be used instead of electricity and is a hopeful option for a sustainable energy environment. Today, natural energy sources like wind, sun, biomass, water, and waves can be used to solve energy problems. But these sources have some problems with how well they work and how much they fluctuate. Even so, hydrogen is one of the most hopeful alternatives, and researchers are very interested in it [13, 14].

Hydrogen has significant potential as an energy carrier that could revolutionize transportation and transform portable applications. To optimize the use of hydrogen as an energy carrier, it is imperative to consider many elements, such as transportation, production, and storage. Several theoretical and experimental studies have been conducted to evaluate the hydrogen storage potential of various alkali metal-based complex hydrides. For instance, Pan and Gao [15] investigated the structural stability, hydrogen storage capacity, and dehydrogenation mechanism of $AMMgH_3$ (AM = Li, Na, K, Rb) hydrides using density functional theory, highlighting their promising characteristics for hydrogen storage applications. Pan and Zhu [16] carried out a comprehensive study on $AMAlH_4$ (AM = Li, Na, K, Rb) hydrides, reporting their high hydrogen storage capacities along with detailed insights into their electronic and optical properties. The hydrogen storage properties of light-element-based hydrides have been extensively investigated. Gao et al. [17] explored the structural stability, hydrogen storage mechanism, and electronic properties of $X_3N_3H_6$ (X = B, C, Al) hydrides using first-principles calculations and demonstrated that these compounds are promising candidates with high gravimetric hydrogen storage capacity. Similarly, Zhu et al. [18] examined different phases of $LiAlH_4$ hydrides and comprehensively analyzed their mechanical, electronic, optical, and dehydrogenation properties. Their study revealed that the formation of $[AlH_4]$ groups plays a crucial role in both structural stability and hydrogen storage capacity. Yang et al. [19] investigated the performance of borophene-based single-atom catalysts (SACs) in the hydrogen evolution reaction (HER) and reported that especially Co- and Ni-doped systems exhibit high catalytic activity with low overpotential. This study highlights the critical importance of developing alternative low-cost and highly efficient catalysts for green hydrogen production. On the other hand, Pan and Zhu [20] explored different phases of potassium aluminum hydride ($KalH_4$) using first-principles calculations and predicted the existence of a novel monoclinic (P2/c) phase. Moreover, this phase was found to possess a hydrogen storage capacity of 5.7 wt%, indicating its potential to meet the U.S. Department of Energy (DOE) targets. These studies provide valuable evidence regarding the applicability of different alkali metal complex hydrides in hydrogen storage technologies, thereby underscoring the significance of investigating $AMGaH_4$ compounds to address the existing gap in the literature.

In 2010, Herbst et al. examined the elastic and thermophysical properties of $AGaH_4$ (A = Li, Na, K, Rb, and Cs) compounds using density functional theory [21]. The structural, electronic, elastic, optical, thermal, and hydrogen storage properties of $XGaH_5$ (X = Ba, Ca, and Mg) were also studied by us in an ab initio study [22]. We selected the alkali metal series (Li, Na, K, Rb, Cs) because they provide a systematic trend in ionic size, electronegativity, and bonding strength, which allows us to clarify the structure–property relationships of $MGaH_4$ hydrides. Lightweight elements such as Li and Na enhance gravimetric hydrogen capacity ($LiGaH_4$ reaches 5.00 wt%, close to the DOE target), while heavier alkalis improve thermodynamic stability. Moreover, alkali metals exhibit strong reactivity and hydrogen affinity, favoring stable hydride formation. This choice is also motivated by the well-established role of alkali-based complex hydrides (e.g., $LiAlH_4$, $NaAlH_4$) in hydrogen storage, whereas gallium-based analogues remain largely unexplored. The only previous theoretical work on $AGaH_4$ compounds was

carried out by Herbst et al. (2010), which focused mainly on elastic and thermo-physical properties without addressing optical, electronic, dynamic, or hydrogen storage characteristics. Our study systematically fills this gap by providing a comprehensive investigation of structural, electronic, mechanical, optical, thermal, and hydrogen storage properties across the alkali series. Although the calculated gravimetric hydrogen storage capacities of $MGaH_4$ hydrides (1.95–5.00 wt%) are slightly below the DOE target of 5.5 wt%, the results remain scientifically significant. $LiGaH_4$ reaches 5.00 wt% and, more importantly, achieves a volumetric capacity of 92.81 gH_2L^{-1}, which far exceeds the DOE target of 40 gH_2L^{-1}. In addition, the relatively low hydrogen desorption temperatures (113.70–183.01 K) indicate favorable thermodynamics for practical applications. This systematic investigation across the alkali series provides valuable insight into how cation size and bonding strength affect hydrogen storage and stability, while also offering a theoretical foundation for further strategies such as doping, alloying, or nanostructuring to enhance storage performance.

The primary objective of this study is to provide a comprehensive investigation of novel materials that can contribute to the safe, efficient, and high-capacity storage of hydrogen, which has a strategic role in today's energy transformation processes. In this context, the structural, electronic, mechanical, optical, phonon, thermal, and hydrogen storage properties of alkali metal gallium hydrides $MGaH_4$ (M = Li, Na, K, Rb, Cs) have been systematically analyzed within the framework of density functional theory (DFT). Although these compounds have been only marginally addressed in the literature, they stand out as promising candidates for hydrogen storage technologies. In this study, detailed insights were obtained regarding their structural stability, band gap characteristics, elastic behavior, optical responses, phonon dispersions, thermal parameters, and hydrogen storage capacities, offering a multidimensional assessment of their potential. Accordingly, the results aim not only to fill the existing gap in theoretical studies but also to provide valuable guidance for future experimental research.

2. Methods

The Siesta Package Program [23] was utilized to analyze many physical characteristics of the $MGaH_4$ (M = Li, Na, K, Rb, Cs) compounds, including their structure, electronic properties, elastic behavior, optical attributes, thermal properties, and hydrogen storage properties. This research was performed using Density Functional Theory. The Perdew-Burke-Ernzerhof (PBE) function [24], which is part of the Generalized Gradient Approximation (GGA), was employed to calculate the exchange–correlation energy. Before commencing the calculations, optimizations were performed on the geometry. The simulation analysis selected structures that exhibited the highest stability and the lowest energy use. The computations were performed on these structures as well. The computations utilized norm-conserving pseudopotentials of the Troullier Martins type [25] for the Li, Na, K, Rb, Cs, Ga, and H atoms. The valence electron configurations of the Li, Na, K, Rb, Cs, Ga, and H atoms in the above systems are $2s^1$, $3s^1$, $4s^1$, $5s^1$, $6s^1$, $4s^2 3d^{10} 4p^1$, $1s^1$, respectively.

The computations were performed with the double zeta polarized basis set. After the optimization process, the mesh cut-off energy value was determined to be 350 Rydberg. The Brillouin zones (BZ) for $MGaH_4$ were separated using a k-point mesh and the Monkhorst–Pack method [26]. The k-point meshes utilized for $LiGaH_4$, $NaGaH_4$, $KGaH_4$, $RbGaH_4$, and $CsGaH_4$ were $8 \times 6 \times 10$, $8 \times 10 \times 6$, $6 \times 10 \times 8$, $6 \times 10 \times 8$, and $6 \times 10 \times 8$, respectively. The conjugate-gradient (CG) approach was employed to optimize the structure until the residual force acting on all atoms was below 0.01 eV/ $Å^{-1}$. The maximal atomic displacements and maximum force were defined as 1.0 Å and 10^{-5} eV/atom, respectively. We utilized the Vesta program [27] to obtain comprehensive data on the compounds analyzed, encompassing their space group, lattice parameter values, and atomic coordination. The second-order independent elastic constant values of $MGaH_4$ were determined using the volume-conserving approach and the Siesta program.

3. Results and discussion

3.1. Structural properties

In Fig. 1, $LiGaH_4$ and $NaGaH_4$ with space group Cmcm (No. 63), $KGaH_4$, $RbGaH_4$, and $CsGaH_4$ with space group Pnma (No. 62) are shown, respectively. The unit cell of $MGaH_4$ (M = Li, Na, K, Rb, Cs) compounds consists of 24 atoms, 4 each of M (Li, Na, K, Rb, Cs) and Ga atoms, and 16 of H atoms. For the compound $LiGaH_4$, the Li, Ga, and H atoms are represented by the following Wyckoff positions: Li at 4c (0, 0.4250, 0.2500), Ga at 4c (0, − 0.1830, 0.2500), H1 at 8f (0, 0.6728, 0.4520), and H2 at 8 g (0.2003, − 0.0557, 0.2500). For the compound $NaGaH_4$, the Na, Ga, and H atoms are represented by the following Wyckoff positions: Na at 4c (0, 0.3438, 0.2500), Ga at 4c (0, − 0.1595, 0.2500), H1 at 8f (0, 0.6908, 0.4290), and H2 at 8g (0.1830, − 0.0131, 0.2500). For the compound $KGaH_4$, the K, Ga and H atoms are represented by the following Wyckoff positions: K at 4c (0.1814, 0.2500,

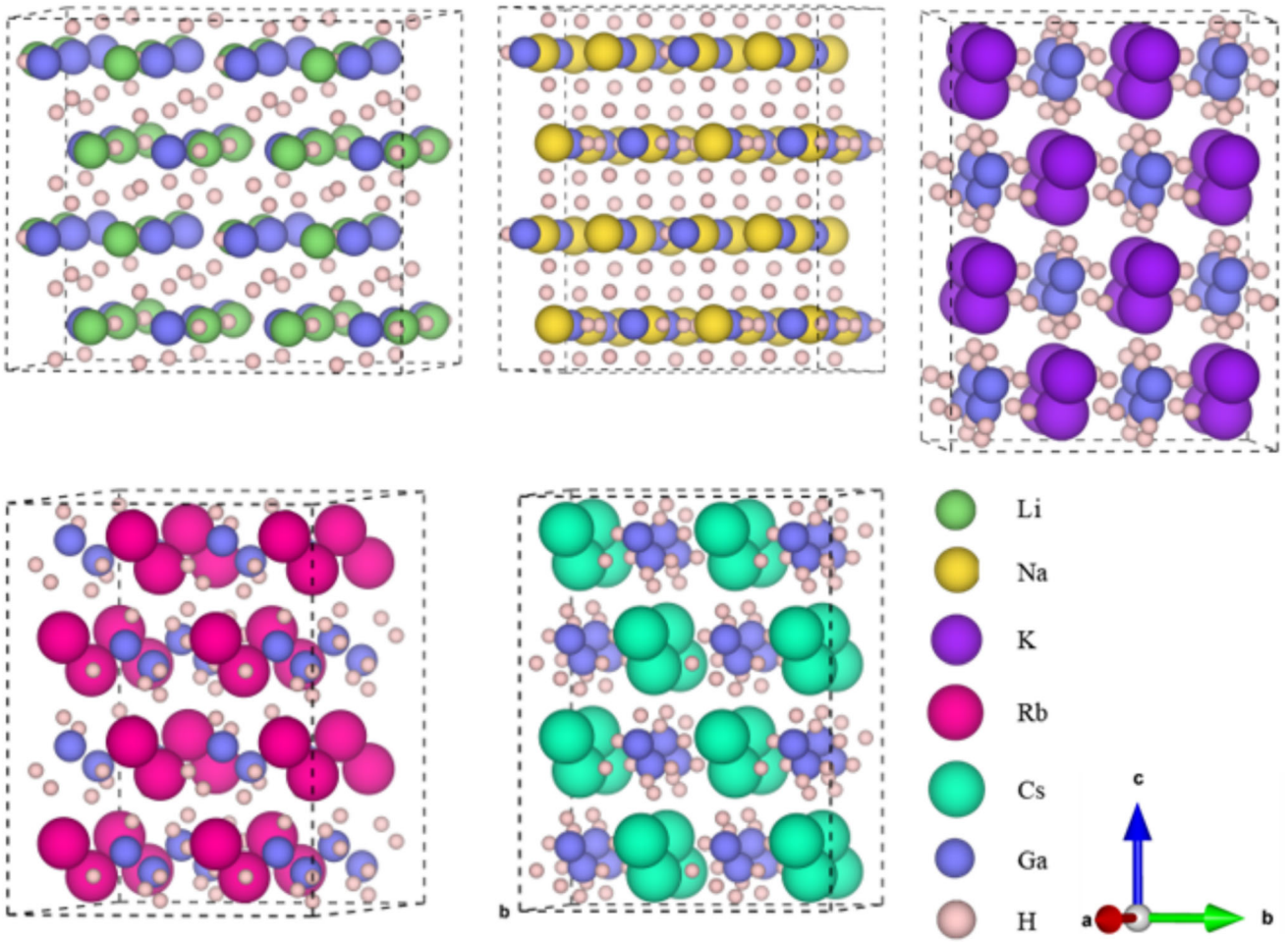

Fig. 1 Systematic representation of 2 × 2 × 2 supercell crystal structures for the $MGaH_4$ (M = Li, Na, K, Rb, Cs) hydrides with crystal axis directions

0.1618), Ga at 4c (0.5628, 0.2500, 0.8091), H1 at 8d (0.4167, 0.9802, 0.3178), H2 at 4c (0.4019, 0.2500, 0.8928), and H3 and 4c (0.6890, 0.2500, 0.9590). For the compound $RbGaH_4$, the Rb, Ga and H atoms are represented by the following Wyckoff positions: Rb at 4c (0.1824, 0.2500, 0.1624), Ga at 4c (0.5621, 0.2500, 0.8071), H1 at 8d (0.4178, 0.9742, 0.3155), H2 at 4c (0.4076, 0.2500, 0.8880), and H3 and 4c (0.6829, 0.2500, 0.9529). For the compound $CsGaH_4$, the Cs, Ga and H atoms are represented by the following Wyckoff positions: Cs at 4c (0.1845, 0.2500, 0.1642), Ga at 4c (0.5600, 0.2500, 0.8038), H1 at 8d (0.4205, 0.9659, 0.3133), H2 at 4c (0.4137, 0.2500, 0.8811), and H3 and 4c (0.6736, 0.2500, 0.9442). All structures were optimized at zero temperature and pressure. The results obtained are presented in Table 1 with unit cell volume, formation energy, and cohesive energy in comparison with other studies in the literature. The results found in Table 1 are consistent with the findings of earlier theoretical investigations in the literature[4, 5].

The average bond lengths and bond angles of the structure optimized for $LiGaH_4$ are Ga-H (1.586–1.618 Å) and H-Ga-H (101.21°–111.27°). The average bond lengths and bond angles of the structure optimized for $NaGaH_4$ are Ga-H (1.601–1.603 Å) and H-Ga-H (106.33°–110.64°). The average bond lengths and bond angles of the structure optimized for $KGaH_4$ are Ga-H (1.594–1.611 Å) and H-Ga-H (109.37°–113.42°). The average bond lengths and bond angles of the structure optimized for $RbGaH_4$ are Ga-H (1.595–1.600 Å) and H-Ga-H (109.51°–113.02°). The average bond lengths and bond angles of the structure optimized for $CsGaH_4$ are Ga-H (1.597–1.612 Å) and H-Ga-H (108.68°–112.72°).

The thermal stability of hydrides is a crucial determinant for their suitability in solid-state hydrogen storage, as it directly impacts the quantity and longevity of hydrogen that can be stored within them. To assess the thermal stability of $MGaH_4$ (M = Li, Na, K, Rb, Cs) hydrides, we conducted measurements to determine their enthalpy of

Table 1 The computed lattice constants (a, b, c (Å)), unit cell volume (V $\left(Å^3\right)$), formation energy (ΔE_f(eV/atom)), and cohesive energy (E_{coh}(eV/atom)) values of $MGaH_4$ (M = Li, Na, K, Rb, Cs) compounds

Material	a	b	c	V	ΔE_f	E_{coh}	References
$LiGaH_4$	6.4941	7.1160	6.1900	286.17	− 0.154	3.173	This study
	6.4751	7.0749	6.1639	282.36	–	–	[21]
	6.5275	7.0384	6.2093	285.27	–	–	[28]
$NaGaH_4$	7.0829	6.4303	7.1545	325.86	− 0.168	3.127	This study
	7.0662	6.4163	7.1387	323.64	–	–	[21]
	7.1102	6.4717	7.1089	327.11	–	–	[28]
$KGaH_4$	9.0529	5.5868	7.3200	370.22	− 0.234	3.127	This study
	9.0956	5.6185	7.3604	376.12	–	–	[21]
	9.1133	5.6467	7.3990	380.75	–	–	[28]
$RbGaH_4$	9.5183	5.7879	7.6396	420.88	− 0.239	3.108	This study
	9.4928	5.7726	7.6179	417.44	–	–	[21]
	9.5390	5.8275	7.6823	427.47	–	–	[28]
$CsGaH_4$	10.0854	6.0219	7.9987	485.79	− 0.248	3.110	This study
	10.0399	5.9992	7.9668	479.84	–	–	[21]
	10.0154	6.0995	7.9831	487.67	–	–	[28]

formation (ΔH_f). The formation energy was calculated using the equation in Eq. 1.

$$\Delta H_f = E_{tot}(MGaH_4) - E_{tot}(M) - E_{tot}(Ga) - 2E_{tot}(H_2) \quad (1)$$

In the formation energy equation, $E_{tot}(MGaH_4)$, $E_{tot}(M)$, $E_{tot}(Ga)$, and $E_{tot}(H_2)$ represent the total energies of M (Li, Na, K, Rb, Cs), Ga, and H_2, respectively. The calculated formation enthalpies for $LiGaH_4$, $NaGaH_4$, $KGaH_4$, $RbGaH_4$, and $CsGaH_4$ are − 0.154, − 0.168, − 0.234, − 0.239, and − 0.248 eV/atom, respectively. The negative value of the formation energy indicates that it is thermodynamically stable and can be synthesized experimentally [29–33]. $CsGaH_4$ was determined to be more stable as a result of its greater negative formation enthalpy energy. The cohesive energy, denoted as E_{coh}, is a fundamental parameter used to assess the stability of a system. The term "bond strength" refers to the amount of energy required to break the atomic bonds within a crystal and separate its distinct components. The magnitude of E_{coh} serves as a measure of the stability of the crystal. Equation 2 below presents the formula for the cohesive energy of the $MGaH_4$ compound.

$$E_{coh} = -\frac{1}{6}[E_{tot}(MGaH_4) - E_{tot}(M) - E_{tot}(Ga) - 2E_{tot}(H_2)] \quad (2)$$

The term $E_{tot}(MGaH_4)$, refers to the total energy of the $MGaH_4$ compound, whereas $E_{tot}(M)$, $E_{tot}(Ga)$, and $E_{tot}(H_2)$ indicate the energy of each atom within the unit cell. The data presented in Table 1 demonstrates that the heat release observed during the process is positive, indicating a shift from isolated atoms to chemical compounds [34]. The results demonstrate the thermodynamic stability of all the materials that were examined.

We can also gain insight into the structural stability of these hydrides based on the formation enthalpy and cohesive energy values provided in Table 1. Formation enthalpy reflects the thermodynamic stability of a compound relative to its constituent elements, while cohesive energy represents the average bond strength within the compound. A more negative ΔHf indicates higher thermodynamic stability, whereas a higher Ecoh corresponds to stronger atomic bonding. In our study, $CsGaH_4$ shows the most negative ΔHf (− 0.248 eV/atom), indicating high thermodynamic stability, while $LiGaH_4$ shows the highest Ecoh (3.173 eV/atom), reflecting strong internal bonding. This correlation suggests that both thermodynamic and bonding stabilities should be considered when evaluating structural robustness.

3.2. Mechanical properties

3.2.1. Single-crystal elastic constant

The mechanical properties of materials, including elasticity, interatomic forces, mechanical features, and phase transition, have a crucial influence on forming different

Table 2 The values of the Kleinman parameter (ζ), tetragonal shear constant (C), elastic constants (C_{ij} in GPa), and Cauchy pressure (C_p in GPa) for the $MGaH_4$ compounds (M = Li, Na, K, Rb, and Cs)

Parameters	$LiGaH_4$	$NaGaH_4$	$KGaH_4$	$RbGaH_4$	$CsGaH_4$	References
C_{11}	48.65	23.73	27.69	17.78	15.83	This study
	46.80	26.50	18.70	17.00	14.70	[21]
C_{22}	17.79	19.86	32.18	18.05	14.55	This study
	14.50	29.50	17.00	15.70	12.60	[21]
C_{33}	35.80	28.61	38.37	20.29	17.94	This study
	34.40	32.20	20.50	20.90	15.70	[21]
C_{44}	12.76	6.68	7.84	6.59	4.24	This study
	13.00	9.20	5.00	5.10	4.70	[21]
C_{55}	10.77	1.80	12.13	4.19	4.37	This study
	10.40	3.50	5.00	5.00	2.70	[21]
C_{66}	7.79	8.66	14.37	11.05	9.76	This study
	10.50	8.50	8.80	9.00	8.20	[21]
C_{12}	2.52	4.09	13.14	5.97	8.98	This study
	4.60	7.10	9.60	9.20	8.70	[21]
C_{13}	7.85	2.46	4.55	2.39	3.18	This study
	8.80	2.60	5.30	4.20	3.50	[21]
C_{23}	4.24	5.15	7.05	3.57	1.25	This study
	5.90	7.40	5.10	3.60	4.30	[21]
$C_P(C_{12}–C_{66})$	− 5.27	− 4.58	− 1.23	− 5.09	− 0.78	This study
C’	23.06	9.82	7.28	5.91	3.42	This study
ζ	0.21	0.36	0.79	0.58	0.94	This study

physical qualities [35]. The mechanical qualities play a vital role in determining the effectiveness of hydrogen storage materials and their practical uses. Elastic constants, denoted as C_{ij}, are fundamental material factors that determine the relationship between mechanical and dynamic properties. They offer valuable insights into the inherent forces present in solids and provide crucial information regarding the stability, rigidity, and bonding characteristics of a material. These factors encompass crucial attributes such as stiffness, brittleness, ductility, elastic anisotropy, and stability, all of which profoundly influence the choice of materials in many engineering applications. The modified Born-Huang stability criterion for the orthorhombic crystal structure is shown in Eq. 3 [36]:

$$C_{11} > 0,\ C_{44} > 0,\ C_{55} > 0,\ C_{66} > 0,\ C_{11}C_{22} > C_{12}^2,$$
$$C_{11}C_{22}C_{33} + 2C_{12}C_{13}C_{23} - C_{11}C_{23}^2 - C_{22}C_{13}^2 - C_{33}C_{12}^2 > 0 \quad (3)$$

Table 2 demonstrates that the elastic constants exhibit no negative values and fulfill the criterion for mechanical stability. This suggests that the $MGaH_4$ (M = Li, Na, K, Rb, Cs) compound possesses mechanical stability. The elastic constants obtained were also compared with other studies available in the literature. The crystal’s resistance to tensile stress along the a, b, and c axes is measured by the three diagonal elastic constants C_{11}, C_{22}, and C_{33}, respectively. For $LiGaH_4$, $NaGaH_4$, and $CsGaH_4$ hydrides, C_{22} is smaller than C_{11} and C_{33}, indicating that these hydrides are more compressible in the b-direction than in the a- and c-directions. For $KGaH_4$ and $RbGaH_4$ hydrides, C_{11} is smaller than C_{22} and C_{33}, indicating that these hydrides are more compressible in the a-direction than in the b- and c-directions.

The elastic constant C_{44} represents the ability of a compound to resist shear deformation when tangential stress is applied to the (100) plane in the [010] direction. It is observed that the C_{44} value for $MGaH_4$ (M = Li, Na, K, Rb, Cs) hydrides is significantly lower than both C_{11} and C_{33}, suggesting that the hydrides are more susceptible to deformation caused by shear stress compared to stress applied in a single direction along any of the three crystallographic orientations. For $LiGAH_4$, the value of C_{66} is lower than that of C_{44}, suggesting that shear deformation along the (001) plane is easier compared to shear deformation along the (100) plane. For $NaGaH_4$, $KGaH_4$, $RbGaH_4$, and $CsGaH_4$, the value of C_{44} is lower than that of C_{66}, suggesting that shear deformation along the (100) plane is easier compared to shear deformation along the

(001) plane. As seen from Table 2, since $C_{11} + C_{22} > C_{33}$, the elastic tensile is higher in the (001) plane than in the c-axis, and the bond in the (001) plane is elastically more rigid than in the c-axis.

The tetragonal shear modulus ($C' = \frac{C_{11}-C_{12}}{2}$), which represents the resistance to shear deformation by shear stress applied in the [1$\bar{1}$0] direction in the (110) plane, is a measure of the stiffness of a crystalline material. The value of C' is directly correlated with the level of dynamic stability exhibited by a crystal. If the shear constant of a material has a positive value, it signifies that the material is stable when subjected to tetragonal distortions. Conversely, if the shear constant is negative, the material is likely to be dynamically unstable. Looking at the C' values in Table 2, it is seen that the values are positive for $MGaH_4$ (M = Li, Na, K, Rb, Cs) hydrides. This is an indication of the mechanical stability of $MGaH_4$ (M = Li, Na, K, Rb, Cs) hydrides.

The Kleinman parameter [37] ($\zeta = \frac{C_{11} + 8C_{12}}{7C_{11} + 2C_{12}}$), a dimensionless parameter, also referred to as the internal strain parameter, is a measure of the stability of the crystal against bending and stretching [38] distortions. Kleinman parameters have values between a minimum value of zero and a maximum value of one. If the value of the Kleinman parameter is close to zero, it means that bond stretching under stress is dominant, and if the value of ζ is close to 1, it means that bond bending is dominant. The calculated Kleinman parameter values for $LiGaH_4$ and $NaGaH_4$ are 0.21 and 0.36. These values suggest that the mechanical strength of these hydrides is dominated by bond stress. The calculated Kleinman parameter value for $RbGaH_4$ hydride is 0.58. According to this value, it is thought that the mechanical strength of $RbGaH_4$ hydride is due to both bond stretching and bond bending. The calculated Kleinman parameter values for $KGaH_4$ and $CsGaH_4$ hydrides are 0.79 and 0.94, respectively. According to these values, it can be said that the mechanical strength of these hydrides is due to bond bending.

Cauchy pressure, another important elastic parameter, provides information about the brittleness or ductility of a material as well as the interatomic bonds. The Cauchy pressure for orthorhombic structures can be obtained from the equations. $C_p = C_{12} - C_{16}$, $C_p = C_{13} - C_{55}$ and $C_p = C_{23} - C_{44}$ [39–41]. A positive value of the Cauchy pressure indicates a metallic bond, while a negative value represents a directional covalent bond of angular character. In addition, a negative value of Cauchy pressure indicates a brittle structure, while a positive value indicates ductility. Therefore, as can be seen from Table 2, the negative Cauchy pressure values calculated for $MGaH_4$ hydrides indicate that these hydrides have a brittle structure and covalent bonding.

3.2.2. *Polycrystalline elastic properties*

For polycrystalline materials, the elastic modulus holds greater significance in terms of practical applicability compared to the elastic constant. The elastic modulus of a material is a physical property that quantifies its ability to resist deformation under tension or compression, as long as it remains within its elastic limit. Poisson's ratio (ν), Young's modulus (E), shear modulus (G), and bulk modulus (B) are typically used to quantify it. Voigt's [42] model and Reuss's [43] model are used in the calculation of elastic moduli. The Voigt model sets an upper bound, while the Reuss model establishes a lower bound for the polycrystalline elastic modulus in the Voigt-Reuss-Hill theory. In contrast, the Hill model determines the arithmetic mean of the Voigt and Reuss models [44]. Bulk modulus $\left(B_H = \frac{B_V+B_R}{2}\right)$ and shear modulus $\left(G_H = \frac{G_V+G_R}{2}\right)$ were defined using the Hill approach. Young's modulus $\left(E = \frac{9GB}{(3B+G)}\right)$ and Poisson's ratio $\left(\nu = \frac{(3B-2G)}{2(3B+G)}\right)$ are calculated using the bulk modulus and shear modulus. All calculated values are given in Table 3. The bulk modulus is highly significant due to its role in assessing the mechanical characteristics of solids. It demonstrates the capacity of solids to withstand compression. As can be seen from Table 3, the fact that the Bulk modulus values for $MGaH_4$ hydrides are larger than the shear modulus values indicates that the mechanical strength will be limited to shear deformation. Young's modulus quantifies the rigidity of an elastic substance in response to a change in its length, and also functions as an indicator of its ability to withstand thermal shock [45]. When the Young's modulus value of a solid material is small, the material is soft. The Young's moduli of all calculated materials have small values, so $MGaH_4$ hydrides are expected to be soft materials.

The B/G ratio, also known as Pugh's ratio, provides information about the brittleness or ductility of a solid material [46–48]. If a material shows ductile properties, the B/G ratio is greater than 1.75. If the B/G ratio is less than 1.75, it exhibits brittle properties. Since the B/G ratio calculated for $MGaH_4$ hydrides is less than 1.75, these hydrides show brittle properties. Poisson's ratio (ν) is an indicator that distinguishes the ductility ($\nu > 0.26$) or brittleness ($\nu < 0.26$) of a solid material. According to this criterion, $LiGaH_4$, $KGaH_4$, $RbGaH_4$, and $CsGaH_4$ are brittle. However, it should be noted that $NaGaH_4$ hydride is on the borderline between brittle and ductile. Poisson's ratio can be used to determine the type of chemical bonding present in solids. The Poisson's ratio is determined to be 0.1 for a covalent solid and 0.33 for a metallic material, as reported in reference [49]. The Poisson's ratio of $MGaH_4$ falls within the range of these two distinct values, suggesting that the chemical bonding in these

Table 3 The calculated values for the polycrystalline B_R, B_V, B_H, bulk moduli, G_R, G_V, G_H, shear moduli, E, Young's modulus (all in GPa), B/G, Pugh's ratio, υ, Poisson's ratio, and μ^M, machinability index for the compounds $MGaH_4$ (M = Li, Na, K, Rb, Cs)

Compound	B_R	B_V	B_H	G_R	G_V	G_H	E	B/G	υ	μ^M	References
$LiGaH_4$	12.00	14.61	13.30	10.82	12.10	11.46	26.71	1.16	0.17	1.04	This Study
	–	–	13.20	–	–	11.20	26.20	–	–	–	[21]
$NaGaH_4$	10.47	10.62	10.54	4.87	7.46	6.17	15.49	1.71	0.26	1.58	This Study
	–	–	13.50	–	–	8.20	20.30	–	–	–	[21]
$KGaH_4$	16.25	16.41	16.33	10.83	11.77	11.30	27.54	1.45	0.19	2.08	This Study
	–	–	10.70	–	–	5.90	15.00	–	–	–	[21]
$RbGaH_4$	8.87	8.88	8.88	6.55	7.31	6.93	16.50	1.28	0.19	1.35	This Study
	–	–	9.70	–	–	5.90	17.70	–	–	–	[21]
$CsGaH_4$	8.17	8.35	8.26	4.93	6.00	5.47	13.44	1.51	0.23	1.95	This Study
	–	–	8.40	–	–	4.40	11.20	–	–	–	[21]

hydrides is a combination of covalent and metallic. Additionally, Poisson's ratio provides further insight into the nature of the bonding forces. The reported range of ν for central-force solids is 0.25–0.50. If ν falls within this range, the solid is considered to have central inter-atomic forces. Otherwise, it is classified as a non-central force solid [50, 51]. Based on this classification, the values of ν for the $NaGaH_4$ compound suggest the presence of central inter-atomic forces, while for $LiGaH_4$, $KGaH_4$, $RbGaH_4$, and $CsGaH_4$, it indicates the involvement of non-central forces in these solids.

Machinability index ($\mu^M = \frac{B}{C_{44}}$), calculated from the ratio of bulk modulus in C_{44}, is a very important parameter in engineering applications where solids are used [52]. Machinability refers to the inherent property of a material that determines its ease of being machined using a cutting tool. A material with exceptional machinability necessitates lower energy use during cutting, yields a pristine surface quality, and minimizes tool deterioration. The machinability index is a commonly utilized metric in the field of engineering for evaluating the ease of machining in manufacturing and production processes. Machinability is influenced by several elements, such as the tool's type and shape, the cutting process, the machine tool, the metallurgical structure of the tool, and the cutting depth. Additionally, it has an impact on the malleability and reduced friction of solid materials. $KGaH_4$ (2.08) exhibits a greater value of μ^M in comparison to $LiGaH_4$ (1.04), $NaGaH_4$ (1.58), $RbGaH_4$ (1.35), and $CsGaH_4$ (1.95). KGaH4 exhibits larger elastic moduli compared to $LiGaH_4$, $NaGaH_4$, $RbGaH_4$, and $CsGaH_4$, suggesting that $KGaH_4$ is more suitable for tool applications than the latter compounds. Among the phases under investigation, $KGaH_4$ has the highest μ^M value of 2.08, while $LiGaH_4$ has the lowest value.

3.2.3. *Hardness*

Hardness is an essential property of solids that are widely utilized in various technological applications. It quantitatively measures a substance's ability to resist deformation, show plasticity, and demonstrate strength [53]. Hardness is instrumental in comprehending the mechanical behavior of solids. The hardness of a solid, which is influenced by its elastic moduli, can be calculated using the following equations [52, 54–57].

$$(H_V)_{miao} = \frac{(1-2\nu)E}{6(1+\nu)} \tag{4}$$

$$(H_V)_{Chen} = 2\left[\left(\frac{G}{B}\right)^2 G\right]^{0.585} - 3 \tag{5}$$

$$(H_V)_{Tian} = 0.92\left(\frac{G}{B}\right)^{1.137} G^{0.708} \tag{6}$$

$$(H_V)_{Teter} = 0.151G \tag{7}$$

$$(H_V)_{Mazhnik} = \gamma_0 \chi(\sigma) E \tag{8}$$

$\chi(\sigma)$ in Eq. 8 is a function of the poison ratio and is calculated as follows:

$$\chi(\sigma) = \frac{1 - 8.5\sigma + 19.5\sigma^2}{1 - 7.5\sigma + 12.2\sigma^2 + 19.6\sigma^3}$$

Also γ_0 is a dimensionless constant with a value of 0.096.

Table 4 The computed hardness (GPa) values of $MGaH_4$ (M = Li, Na, K, Rb, Cs) compounds

Compound	$(H_V)_{Chen}$	$(H_V)_{Tian}$	$(H_V)_{Teter}$	$(H_V)_{Miao}$	$(H_V)_{Mazhnik}$	$(H_V)_{avg}$
$LiGaH_4$	4.00	4.25	1.73	2.56	1.80	2.87
$NaGaH_4$	0.10	1.65	0.93	1.01	0.73	0.88
$KGaH_4$	2.37	3.16	1.71	2.12	1.31	2.13
$RbGaH_4$	1.65	2.62	1.05	1.43	0.94	1.54
$CsGaH_4$	0.33	1.78	0.83	0.99	0.62	0.91

The $(H_V)_{miao}$, $(H_V)_{Chen}$, $(H_V)_{Tian}$, $(H_V)_{Teter}$, and $(H_V)_{Mazhnik}$ values obtained for the $MGaH_4$ (M = Li, Na, K, Rb, Cs) compounds are presented in Table 4.

The hardness values obtained by various methods exhibit disparities. The expectation arises from the fact that the formulas were developed using distinct elastic moduli (either shear modulus or both shear modulus and bulk modulus and Young's modulus) and Poisson's ratio. Mazhnik et al. [57] said that there can be significant variations in hardness ratings when computed based on the elastic moduli of materials. We calculated the average hardness values of $MGaH_4$ (M = Li, Na, K, Rb, Cs) compounds to estimate their hardness. The average hardness ($(H_V)_{avg}$) values for $MGaH_4$ (M = Li, Na, K, Rb, Cs) hydrides were obtained as 2.87, 0.88, 2.13, 1.54, and 0.91, respectively, and the order is $LiGaH_4 > KGaH_4 > RbGaH_4 > CsGaH_4 > NaGaH_4$. The measured hardness values range from 0.88 to 2.87 GPa, indicating that all the compounds being studied are classified as soft.

3.2.4. *Elastic anisotropy*

Elastic anisotropy impacts various mechanical phenomena, such as the development of plastic deformations in crystals, the displacement of fractures in materials, and the production of cracks in materials. An anisotropic material exhibits varying physical properties in different directions. Comprehending elastic anisotropy has substantial implications for both practical engineering disciplines and the study of crystal physics. Therefore, it is crucial to thoroughly calculate the elastic anisotropy characteristics of $MGaH_4$ (M = Li, Na, K, Rb, Cs) compounds to gain a deeper understanding of their flexibility and potential uses in various external stress conditions. In this section, calculations of shear anisotropy factors ($A_{1,2,3}$), shear modulus percent anisotropy factor (A_G), bulk modulus percent anisotropy factor (A_B), Zener anisotropy (A^{eq}), linear compressibility (K_c/K_a), universal anisotropy index (A^U, d_E) and universal log-Euclidean index (A^L) for $MGaH_4$ (M = Li, Na, K, Rb, Cs) compounds are presented. Shear anisotropy factors for an orthorhombic crystalline system are obtained by the following equations.[58, 59].

Shear anisotropy factor between $\langle 011 \rangle$ and $\langle 010 \rangle$ directions for shear plane {100},

$$A_1 = \frac{C_{44}}{(C_{11} + C_{33} + -2C_{13})} \tag{9}$$

Shear anisotropy factor between $\langle 101 \rangle$ and $\langle 001 \rangle$ directions for shear plane {010},

$$A_2 = \frac{4C_{55}}{C_{22}+C_{33} - 2C_{23}} \tag{10}$$

Shear anisotropy factor between $\langle 110 \rangle$ and $\langle 010 \rangle$ directions for shear plane {001},

$$A_3 = \frac{4C_{66}}{(C_{11} + C_{22} + -2C_{12})} \tag{11}$$

The shear anisotropy factors calculated for $MGaH_4$ hydrides are listed in Table 5.

A_1, A_2, and A_3 values equal to 1 indicate isotropy, while values different from 1 indicate anisotropy. Therefore, $MGaH_4$ hydrides exhibit anisotropic properties. Regarding A_1, $RbGaH_4$ exhibits the lowest level of anisotropy, while $KGaH_4$ displays the highest level of anisotropy. Regarding A_2, $LiGaH_4$ exhibits the lowest level of anisotropy,

Table 5 Shear anisotropy factors (A_1, A_2, A_3), compressibility anisotropy (A_B), shear anisotropy (A_G), universal anisotropy index (A^U), equivalent Zener anisotropy measure (A^{eq}), universal log-Euclidean index (A_L) and linear compressibility ratio (K_c/K_a) for the hydrides $MGaH_4$ (M = Li, Na, K, Rb, Cs)

Parameters	$LiGaH_4$	$NaGaH_4$	$KGaH_4$	$RbGaH_4$	$CsGaH_4$
A_1	0.742	0.563	0.551	0.792	0.620
A_2	0.955	0.189	0.860	0.537	0.584
A_3	0.507	0.978	1.710	1.851	3.148
A_B	0.098	0.007	0.005	0.001	0.011
A_G	0.056	0.210	0.042	0.055	0.098
A^U	0.812	2.670	0.446	0.583	1.108
d_E	2.610	2.944	2.539	2.566	2.666
A^{eq}	2.228	3.973	1.981	1.981	2.528
A^L	0.553	0.231	0.019	0.019	0.077
K_c/K_a	1.269	0.876	1.059	1.059	1.250

whereas $NaGaH_4$ displays the highest level of anisotropy. Regarding A_3, $NaGaH_4$ exhibits the lowest degree of anisotropy, whereas $CsGaH_4$ displays the highest degree of anisotropy.

The equations presented are employed to determine the universal anisotropy index (A^U and d_E), the Zener anisotropy measure (A^{eq}), shear anisotropy (A_G), and compressibility anisotropy (A_B) for materials exhibiting any crystal symmetry [60–63].

$$A^U = \frac{B_V}{B_R} + 5\frac{G_V}{G_R} - 6 \geq 0 \tag{12}$$

$$d_E = \sqrt{A^U + 6} \tag{13}$$

$$A^{eq} = \left(1 + \frac{5}{12}A^U\right) + \sqrt{\left(1 + \frac{5}{12}A^U\right)^2 - 1} \tag{14}$$

$$A_B = \frac{B_V - B_R}{B_V + B_R} \tag{15}$$

$$A_G = \frac{G_V - G_R}{G_V + G_R} \tag{16}$$

A commonly used metric in elastic properties to measure anisotropic is the universal anisotropy index A^U. It is a unique anisotropy scale that is independent of the crystal symmetries of solids. The difference between the universal anisotropy index and other anisotropy scales is that it considers both bulk and shear contributions. When the value of the universal anisotropy index is 1, the compound is isotropic, otherwise, it is anisotropic. The A^U values calculated for $MGaH_4$ hydrides are different from 1, as indicated in Table 5, and therefore these hydrides are anisotropic. Once again, it can be noted from Table 5 that the value of the equivalent Zener anisotropy index (A^{eq}) is greater than one, which further confirms the anisotropic characteristics of the compounds. The values of shear anisotropy (A_G) and compressibility anisotropy (A_B) are equal to one for an isotropic crystal, while a value of zero indicates maximum anisotropy. For $NaGaH_4$, $KGaH_4$, $RbGaH_4$, and $CsGaH_4$ hydrides, the shear anisotropy is larger than the compressibility anisotropy, but for $LiGaH_4$ hydride, the compressibility anisotropy is larger than the shear anisotropy.

The log-Euclidean (A^L) formula is defined by the following equation [59]:

$$A^L = \sqrt{\left[\ln\left(\frac{B_V}{B_R}\right)\right]^2 + 5\left[\ln\left(\frac{C_{44}^V}{C_{44}^R}\right)\right]^2} \tag{17}$$

The constants $C_{44}^V = \frac{3}{5}\frac{(C_{11}-C_{12}-2C_{44})}{3(C_{11}-C_{12})+4C_{44}}$ and $C_{44}^R = \frac{5}{3}\frac{C_{44}(C_{11}-C_{12})}{3(C_{11}-C_{12})+4C_{44}}$ are the Voigt and Reuss approximations for the elastic constant C_{44}, respectively. According to Kube and Jong [60, 64], the A^L value for inorganic crystals spans from 0 to 10.26, with approximately 90% of compounds having an A^L value of less than one. Furthermore, a significant proportion (78%) of inorganic crystalline compounds with high A^L values display layered or lamellar structures [65]. High values of A^L suggest a pronounced layered structure, whereas low values of A^L indicate a structure that lacks layering. The low A^L value suggests that $MGaH_4$ (M = Li, Na, K, Rb, Cs) does not possess clearly defined layered features. When perfect isotropy is achieved, the value of A^L is precisely zero. The A^L values for the molecules $LiGaH_4$, $NaGaH_4$, $KGaH_4$, $RbGaH_4$, and $CsGaH_4$ are predicted to be 0.553, 0.231, 0.019, 0.019, and 0.077, respectively. All these numbers are below 1, indicating a moderate level of anisotropy.

The computation of linear compressibility along the a and c axes is determined using the following equation [66].

$$\frac{k_c}{k_a} = f = \frac{C_{11} + C_{12} - 2C_{13}}{C_{33} - C_{13}} \tag{18}$$

The f-value is a crucial determinant that determines whether a material exhibits isotropy or anisotropy. An isotropic material is defined as having a f value of one. If the value of f is not equal to one, it indicates that the material exhibits anisotropy. The data presented in Table 5 demonstrates that the $MGaH_4$ (M = Li, Na, K, Rb, Cs) hydrides exhibit anisotropic characteristics. The data presented in Table 5 is unique and does not have any current estimates available for comparison.

The equations that define the bulk modulus along the a, b, and c axes and their anisotropies are as follows [59]:

$$B_a = a\frac{dP}{da} = \frac{\mathrm{D}}{1 + \alpha + \beta}, \quad B_b = b\frac{dP}{db} = \frac{B_a}{\alpha}, \quad B_c = c\frac{dP}{dc} = \frac{B_a}{\beta} \tag{19}$$

where $\mathrm{D} = C_{11} + 2C_{12}\alpha + C_{22}\alpha^2 + 2C_{13}\beta + C_{33}\beta^2 + 2C_{23}\alpha\beta$ and

$$\alpha = \frac{\{(C_{11} - C_{12})(C_{33} - C_{13})\} - \{(C_{23} - C_{13})(C_{11} - C_{13})}{\{(C_{33} - C_{13})(C_{22} - C_{12})\} - \{(C_{13} - C_{23})(C_{12} - C_{23})\}}$$

$$\beta = \frac{\{(C_{22} - C_{12})(C_{11} - C_{13})\} - \{(C_{11} - C_{12})(C_{23} - C_{12})\}}{\{(C_{22} - C_{12})(C_{33} - C_{13})\} - \{(C_{12} - C_{23})(C_{13} - C_{23})\}}$$

The B_b and B_c values of the $LiGaH_4$ and $CsGaH_4$ hydrides are much lower than the B_a value. Accordingly, it is harder for the $LiGaH_4$ and $CsGaH_4$ hydrides to compress in the a direction than in the b and c directions. For the $NaGaH_4$, $KGaH_4$, and $RbGaH_4$ hydrides, the B_c value is higher than the B_a and B_b values. These findings indicate that the ability of the $NaGaH_4$, $KGaH_4$, and $RbGaH_4$ hydrides to be compressed is more challenging in the c direction compared to the a and b directions. The information presented in Table 6 is original and does not have any previous data for comparison in the literature. In

Table 6 Bulk moduli B_a, B_b, and B_c in GPa along crystallographic axes a, b, and c, respectively

Compound	B_a	B_b	B_c	α	β	A_{B_a}	A_{B_c}
$LiGaH_4$	74.92	22.58	41.10	3.32	1.82	3.318	1.820
$NaGaH_4$	29.40	26.38	42.59	1.11	0.69	1.115	1.614
$KGaH_4$	37.27	56.55	60.76	0.66	0.61	0.659	1.074
$RbGaH_4$	23.83	27.00	30.35	0.88	0.79	0.883	1.124
$CsGaH_4$	34.46	18.44	27.66	1.87	1.25	1.869	1.500

The linear bulk modulus anisotropies (A_{B_a}, and A_{B_c}) along the a and c axes for $MGaH_4$ (M = Li, Na, K, Rb, Cs) hydrides

addition, as seen in Table 6, the bulk modulus along the a ($A_{B_a} = \frac{B_a}{B_b}$) and c ($A_{B_c} = \frac{B_c}{B_b}$) axes are considered. For $MGaH_4$ (M = Li, Na, K, Rb, Cs) hydrides, both A_{B_a} values and A_{B_c} values do not equal 1, indicating the presence of anisotropy in the axial bulk modulus.

To provide a more comprehensive representation of elastic anisotropy, we utilized the VELAS [67] code to estimate the direction-dependent variation of bulk modulus, shear modulus, Young's modulus, Poisson's ratio, linear compressibility, and hardness. Figures 2 and 3 depict a 3D graph illustrating Young's modulus, bulk modulus, shear modulus, Poisson's ratio, linear compressibility, and hardness. Isotropic crystals should display spherical symmetry in their 3D contour plots. Any deviation from this indicates the presence of anisotropy. Figures 2 and 3 exhibit non-spherical deviations in the 3D depictions of Young's modulus, bulk modulus, shear modulus, Poisson's ratio, linear compressibility, and hardness, demonstrating anisotropy. Table 7 presents the uppermost and lowermost values of Young's modulus, linear compressibility, bulk modulus, and shear modulus, together with their respective ratios. These ratios are useful indicators of elastic anisotropy.

3.3. Optical properties

The optical properties of a material play a vital role in understanding its interaction with light, including reflection, refraction, absorption, scattering, and transmission. Various energy-dependent optical parameters, such as the energy loss function, reflectivity, optical conductivity, refractive index, absorption coefficient, and dielectric function, help predict the overall optical response of a material. In recent years, there has been a growing interest in studying the optical characteristics of materials due to their significance in integrated optics applications. These properties are essential for advancements in optoelectronics, optical modulation, optical information processing, display technologies, communications, and data storage. By analyzing the frequency-dependent optical behavior, researchers can gain insights into aspects such as energy band structures, excitons, localized defects, lattice vibrations, impurity states, and specific magnetic excitations [68]. The frequency-dependent dielectric function was used to calculate the optical characteristics of $MGaH_4$ (M = Li, Na, K, Rb, Cs).

$$\varepsilon(\omega) = \varepsilon_1(\omega) + i\varepsilon_2(\omega) \tag{20}$$

The dielectric function of a material is composed of a real part and an imaginary part, each of which provides a different insight into the optical behaviour of the material. The real part is associated with the degree of polarisation

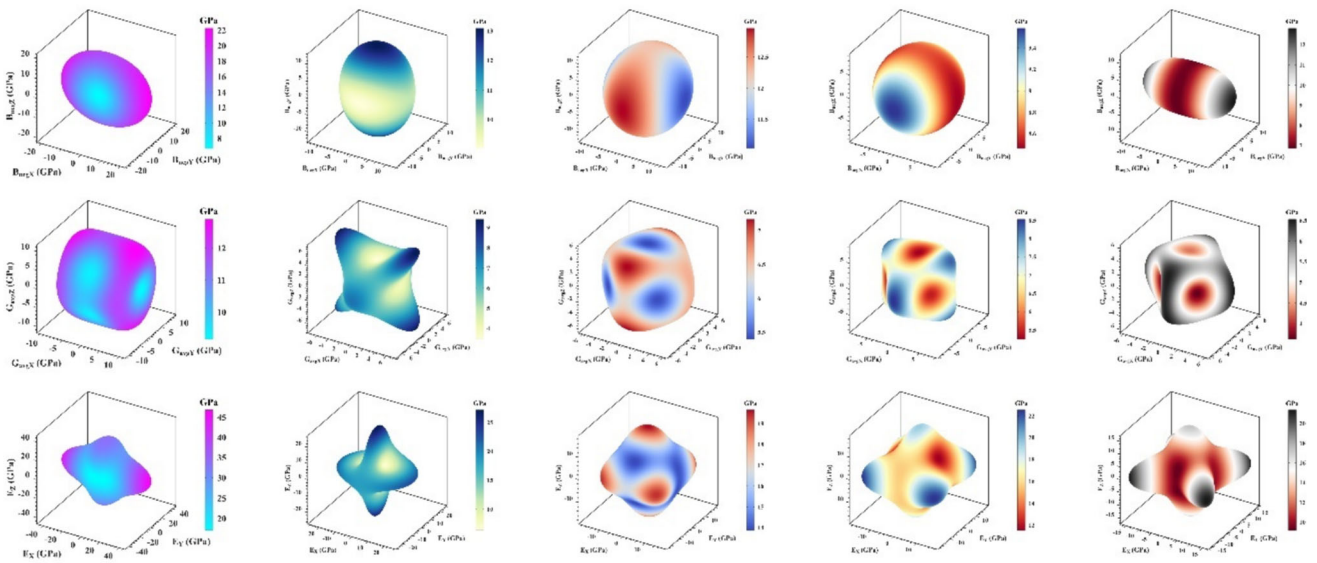

Fig. 2. 3D directional dependences of bulk modulus, shear modulus, and Young's modulus for $MGaH_4$ (M = Li, Na, K, Rb, Cs) hydrides

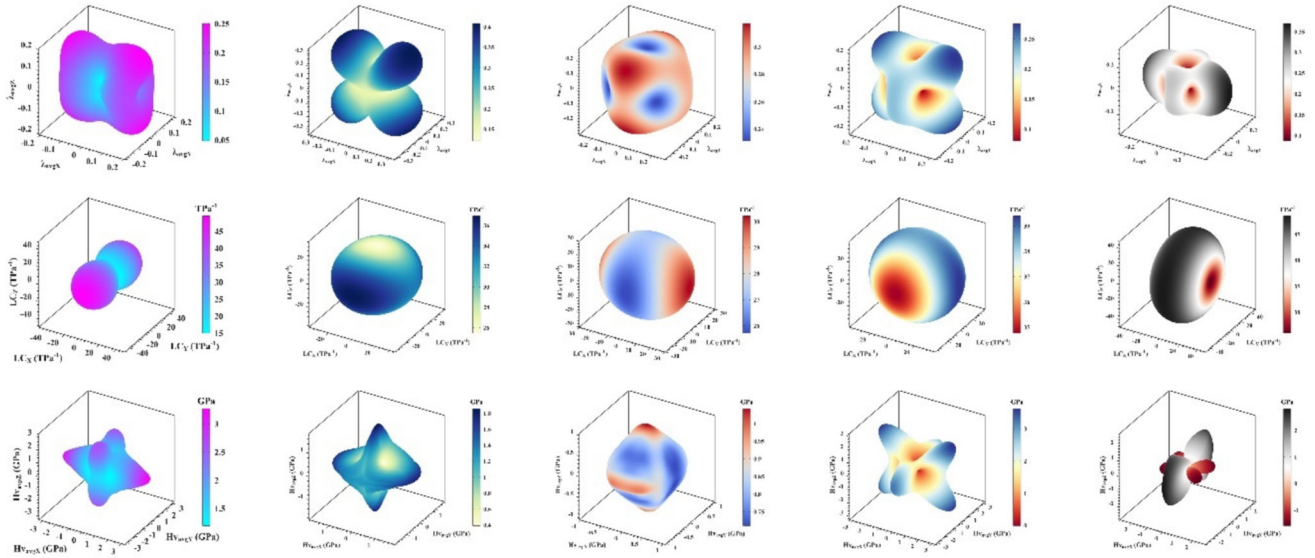

Fig. 3. 3D directional dependences of Poisson's ratio, linear compressibility, and hardness for $MGaH_4$ (M = Li, Na, K, Rb, Cs) hydrides

Table 7 Maximum, minimum, and anisotropy values of Young's modulus, linear compressibility, shear modulus values, and bulk modulus for $MGaH_4$ (M = Li, Na, K, Rb, Cs) hydrides

Compound	E_{min}	E_{max}	A_E	β_{min}	β_{max}	A_β	G_{min}	G_{max}	A_G	B_{min}	B_{max}	A_B
$LiGaH_4$	17.12	46.78	0.21	14.96	49.61	0.35	7.79	16.68	0.13	6.72	22.29	0.28
$NaGaH_4$	6.34	27.18	0.37	25.46	36.93	0.12	1.80	11.74	0.41	9.02	13.09	0.11
$KGaH_4$	21.39	36.70	0.15	16.48	25.00	0.09	7.84	16.63	0.16	13.33	20.23	0.09
$RbGaH_4$	11.53	22.54	0.14	34.77	39.39	0.30	4.19	11.05	0.19	8.46	9.59	0.03
$CsGaH_4$	9.18	21.38	0.19	26.00	48.58	0.14	3.05	9.76	0.22	6.86	12.82	0.18

and the propagation velocity of electromagnetic waves within the material, while the imaginary part reflects the ability of the material to absorb energy from an external electromagnetic field due to frequency-dependent dipole oscillations. Both intraband and interband electronic transitions affect ε(ω) in condensed matter systems. At lower energies, intraband transitions dominate, while interband contributions are largely governed by electronic band structure [69]. Several key optical parameters, including the refractive index, absorption coefficient, energy-loss function, reflectivity, and optical conductivity, can be derived from the complex dielectric function ε(ω), which varies with energy. Figures 4 and 5 illustrate the optical response of $MGaH_4$ (M = Li, Na, K, Rb, Cs) for photon energies up to 25 eV, specifically for the [100] polarization direction of the electric field. Here, ε_1 and ε_2 denote the real and imaginary parts of the dielectric function, respectively. This function characterizes the material's ability to sustain an electromagnetic field [70] and its interaction with incident light, including absorption behavior [71].

The value of the static dielectric function $\varepsilon_1(0)$ is 2.70, 3.28, 3.03, 2.74, and 2.35 for $LiGaH_4$, $NaGaH_4$, $KGaH_4$, $RbGaH_4$, and $CsGaH_4$, respectively. This suggests that the polarizability of $NaGaH_4$ is higher. From Figs. 6(a) and 6(e), the maximum values of $\varepsilon_1(\omega)$ are found to be at 5.74 at 5.03 eV for $LiGaH_4$, 6.90 at 5.04 eV for $NaGaH_4$, 6.67 at 5.36 eV for $KGaH_4$, 6.07 at 5.60 eV for $RbGaH_4$, and 5.24 at 5.84 eV for $CsGaH_4$. In the negative region, the real part $\varepsilon_1(\omega)$ reaches a minimum value of − 0.82 for $LiGaH_4$, − 1.52 for $NaGaH_4$, − 0.65 for $KGaH_4$, − 0.44 for $RbGaH_4$, and − 0.30 for $CsGaH_4$ at photon energies of 7.28, 7.52, 8.24, 8.00, and 9.84 eV, respectively.

The refractive index, denoted as n(ω), is a statistical parameter used to quantify the degree of light refraction. It is particularly useful in the field of photoelectricity. It consists mostly of both actual and imagined components. n(ω) represents the real component, which is commonly referred to as the refractive index. From the Fig. 4(f), the static refractive index n(0) at zero frequency is 1.64 for $LiGaH_4$, 1.81 for $NaGaH_4$, 1.74 for $KGaH_4$, 1.65 for $RbGaH_4$ and 1.53 for $CsGaH_4$. Equation $\varepsilon_1(0) = n^2(0)$

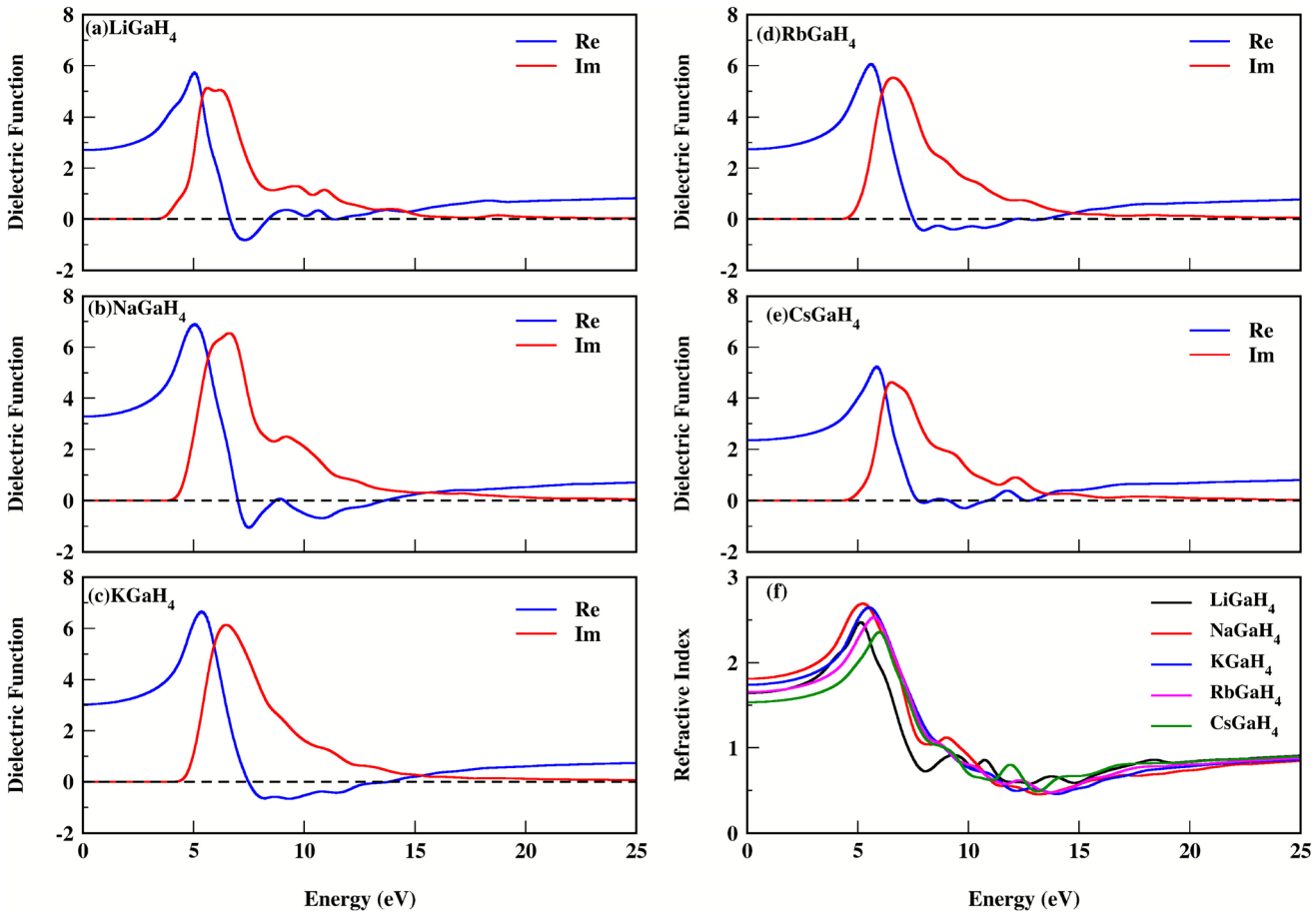

Fig. 4 (**a**)–(**e**) Real and imaginary part of the dielectric function and (**f**) Refractive index for $MGaH_4$ (M = Li, Na, K, Rb, Cs)

shows that these static values of n(0) are comparable with static values of $\varepsilon_1(0)$. The refractive index, n(ω), exhibits an upward trend in the ultraviolet region and attains its maximum value at certain energy levels for different compounds: 2.47 at 5.12 eV for $LiGaH_4$, 2.69 at 5.20 eV for $NaGaH_4$, 2.65 at 5.52 eV for $KGaH_4$, 2.53 at 5.76 eV for $RbGaH_4$, and 2.36 at 6.00 eV for $CsGaH_4$. The higher value of n(ω) for $NaGaH_4$ implies a substantial slowing down of light waves caused by electric polarization, leading to an increased refractive index.

The impact of photons of different frequencies on the conductivity of compounds is represented by the optical conductivity σ(ω), which is displayed in Fig. 5(a). Maximum values of the peaks of σ(ω) are obtained at 426,171 Ω^{-1} cm^{-1} at 6.36 eV for $LiGaH_4$, 589,430 Ω^{-1} cm^{-1} at 6.76 eV for $NaGaH_4$, 543,441 Ω^{-1} cm^{-1} at 6.72 eV for $KGaH_4$, 500,166 Ω^{-1} cm^{-1} at 6.88 eV for $RbGaH_4$, and 413,640 Ω^{-1} cm^{-1} at 7.00 eV for $CsGaH_4$. Moreover, the value of σ(ω) falls with increasing photonic energy after 8 eV. Furthermore, evident is the fact that the compounds' optical conduction only occurs in the UV area and is not common in the visible range. This shows that the compound's electrons would not be excited by incident photons in the visible area.

The absorption coefficient α(ω) quantifies the compounds' ability to absorb incoming photons. Absorption is the phenomenon that happens when the energy of incoming photons matches the transition frequency of the electrons in atoms. Figure 5(b) depicts the absorption coefficient α(ω). Figure 5(b) indicates that the movement of electrons from the valence band to the conduction band is caused by the absorption of photons of different frequencies. In the visible region, the value of the absorption coefficient is zero, which means that there is no optical excitation in this region. The absorption coefficient reaches a maximum at 10.0×10^5 cm^{-1} at 6.72 eV for $LiGaH_4$, 12.6×10^5 cm^{-1} at 7.2 eV for $NaGaH_4$, 12.0×10^5 cm^{-1} at 7.84 eV for $KGaH_4$, 11.4×10^5 cm^{-1} at 7.68 eV for $RbGaH_4$, and 13.1×10^5 cm^{-1} 1 at 7.36 eV for $CsGaH_4$. The abundance of peaks in the higher photon energy range of 6–15 eV indicates that these compounds effectively absorb light in the ultraviolet region.

Reflectivity R(ω) refers to the amount of incident light that is reflected from the compound's surface. The static

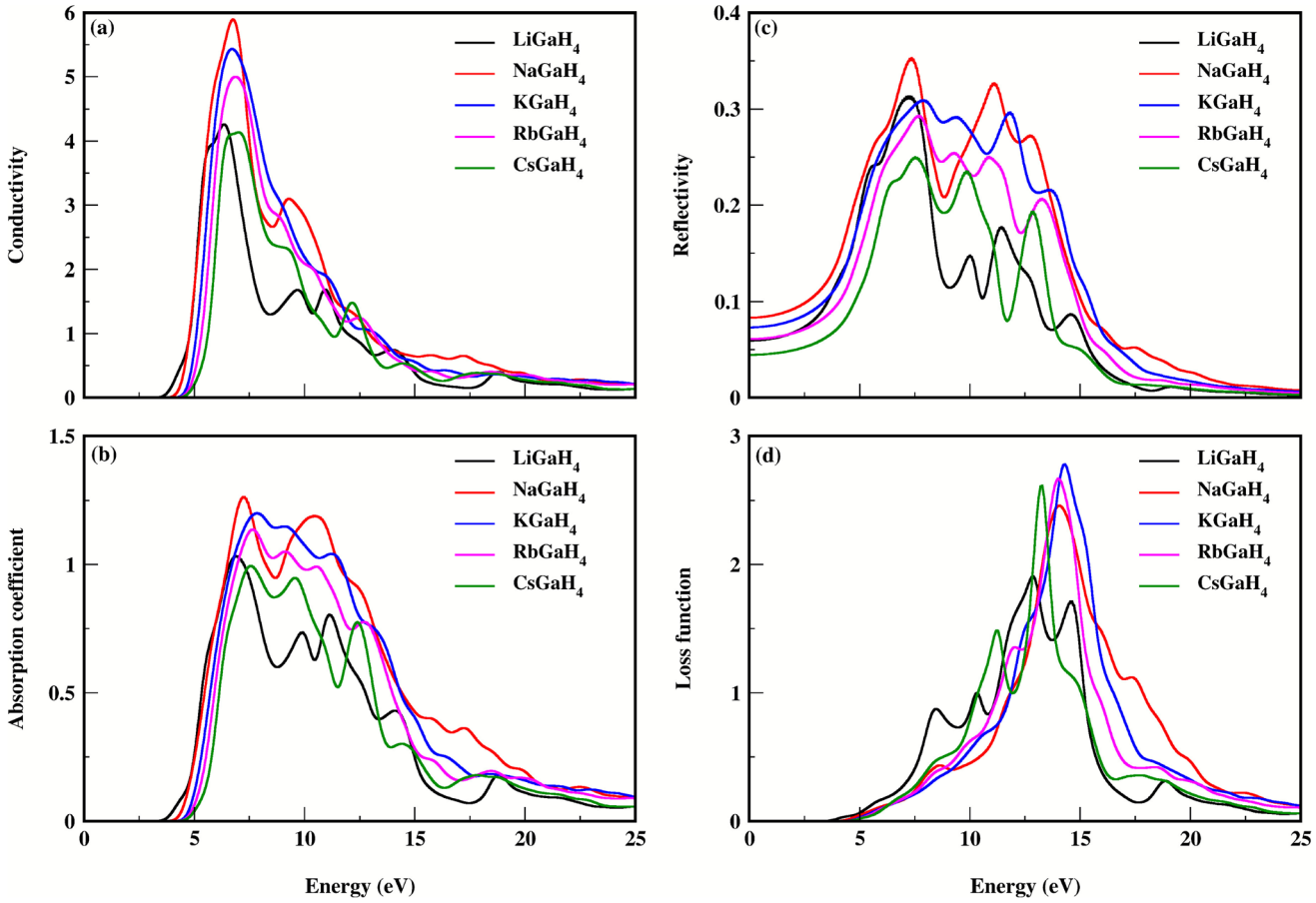

Fig. 5 (**a**) Conductivity, (**b**) Absorption coefficient, (**c**) Reflectivity, and (**d**) Loss function for $MGaH_4$ (M = Li, Na, K, Rb, Cs)

reflectance values R(0) obtained from Fig. 5(c) are 6% for $LiGaH_4$, 8% for $NaGaH_4$, 7% for $KGaH_4$, 6% for $RbGaH_4$ and 4% for $CsGaH_4$. The maximum reflectance R(ω) is observed at 31% at 7.20 eV for $LiGaH_4$, 36% at 7.36 eV for $NaGaH_4$, 31% at 7.84 eV for $KGaH_4$, 29% at 7.76 eV for $RbGaH_4$, and 25% at 7.60 eV for $CsGaH_4$. The reflectivity R(ω) values obtained from Fig. 5(c) indicate that the compounds demonstrate high reflectance in the UV area and low reflection in the visible range.

The energy loss function, L(ω), provides valuable insights into a material's electronic structure, plasmon resonance, absorption characteristics, and reflectivity [72, 73]. This characteristic also determines the amount of energy dissipated when a high-speed electron passes through the material. Moreover, the plasma frequency of a substance is linked to the highest point of L(ω). Figure 5(d) displays the L(ω) spectra of $MGaH_4$ (M = Li, Na, K, Rb, Cs) hydrides. L(ω) values increase in the ultraviolet region at higher frequencies, peaking at 1.90 at 12.92 eV for $LiGaH_4$, 2.46 at 14.00 eV for $NaGaH_4$, 2.78 at 14.32 eV for $KGaH_4$, 2.67 at 14.00 eV for $RbGaH_4$, and 2.61 at 13.28 eV for $CsGaH_4$.

3.4. Electronic properties

The PBE-GGA method is used in this study to determine the band structure and density of states (DOS) of the alkali gallium hydrides $MGaH_4$ (M = Li, Na, K, Rb, Cs). Band structure plots describe the energy levels available for electrons to occupy in a material, allowing for the prediction of the electronic properties of a crystal structure. The band structure and density of states graphs of $MGaH_4$ compounds are shown in Fig. 6. As can be seen from Fig. 6(a), (b), and (e), the maximum point of the valence band and the minimum points of the conduction band for $LiGaH_4$, $NaGaH_4$, and $CsGaH_4$ are at the Γ point in these compounds. Therefore, $LiGaH_4$, $NaGaH_4$, and $CsGaH_4$ have a direct band gap. However, $KGaH_4$ and $RbGaH_4$ hydrides have an indirect band gap because the maximum point of the valence band and the minimum point of the conduction band are not located at the same point. The band gaps for the calculated hydrides were obtained as 4.57 eV for $LiGaH_4$, 4.68 eV for $NaGaH_4$, 5.00 eV for $KGaH_4$, 5.00 eV for $RbGaH_4$, and 4.93 eV for $CsGaH_4$. According to these results, it is seen that alkaline gallium hydrides $MGaH_4$ (M = Li, Na, K, Rb, Cs) have wide band

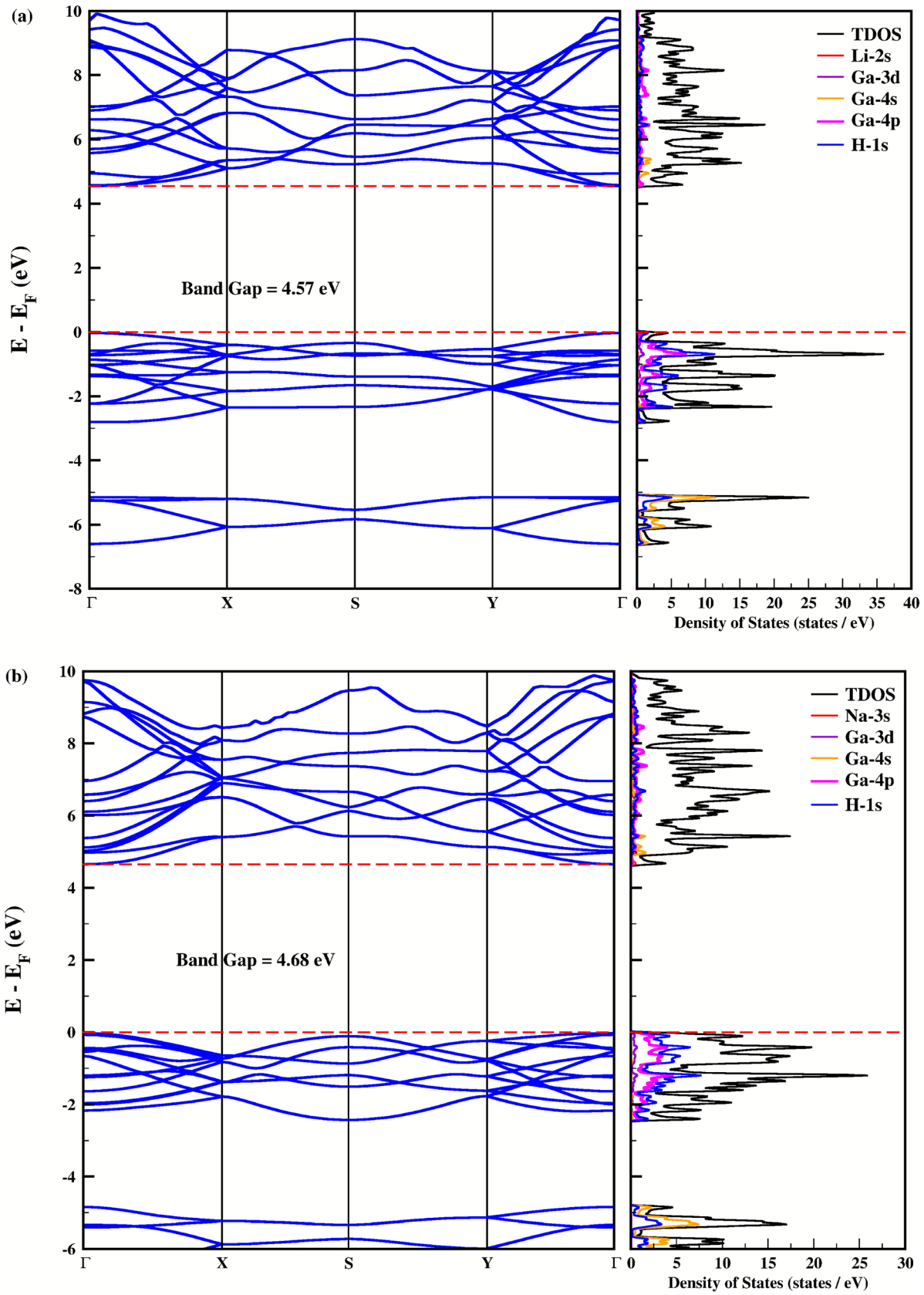

Fig. 6 The calculated band structures and density of states graphs for (**a**) $LiGaH_4$, (**b**) $NaGaH_4$, (**c**) $KGaH_4$, (**d**) $RbGaH_4$, and (**e**) $CsGaH_4$

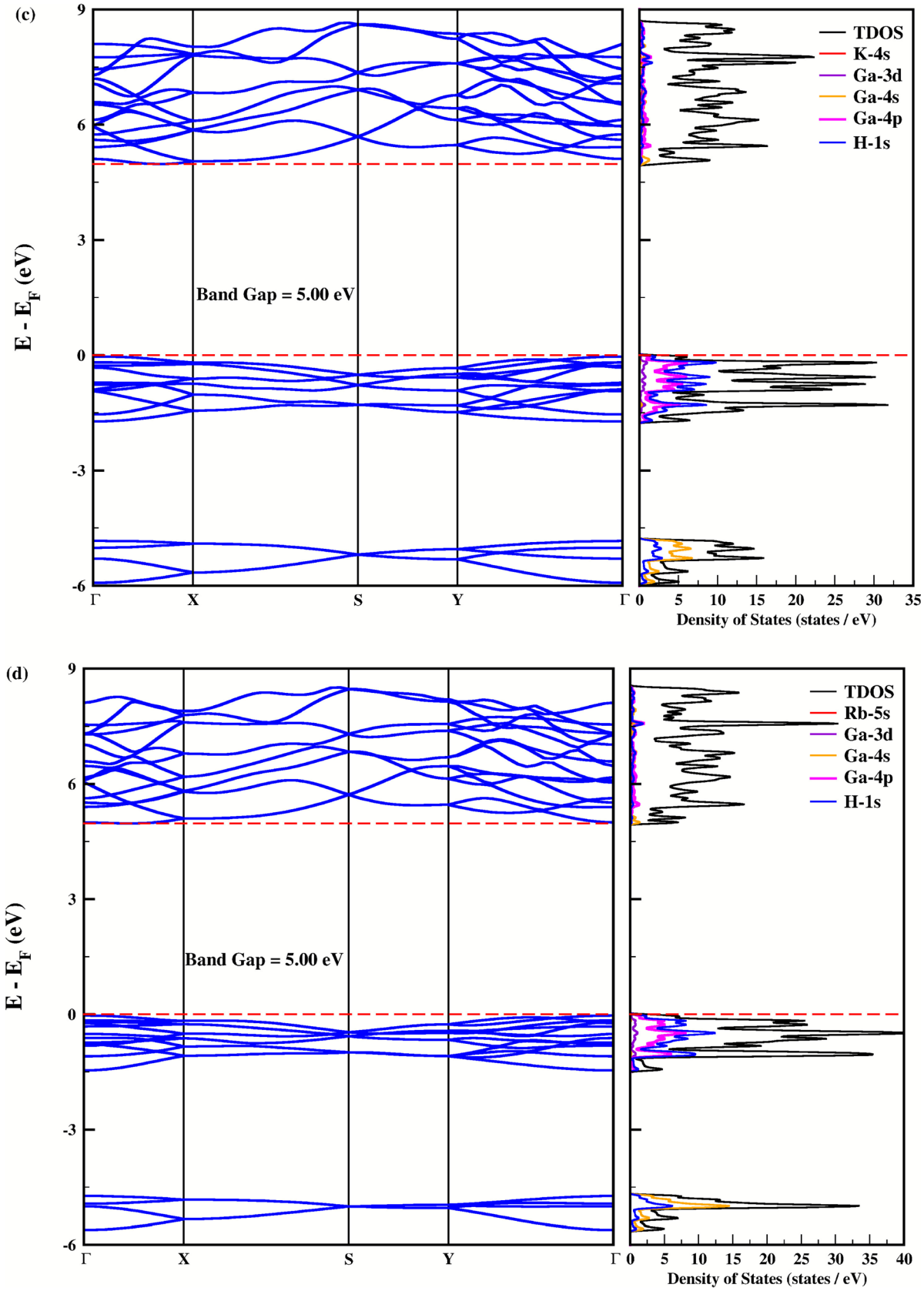

Fig. 6 continued

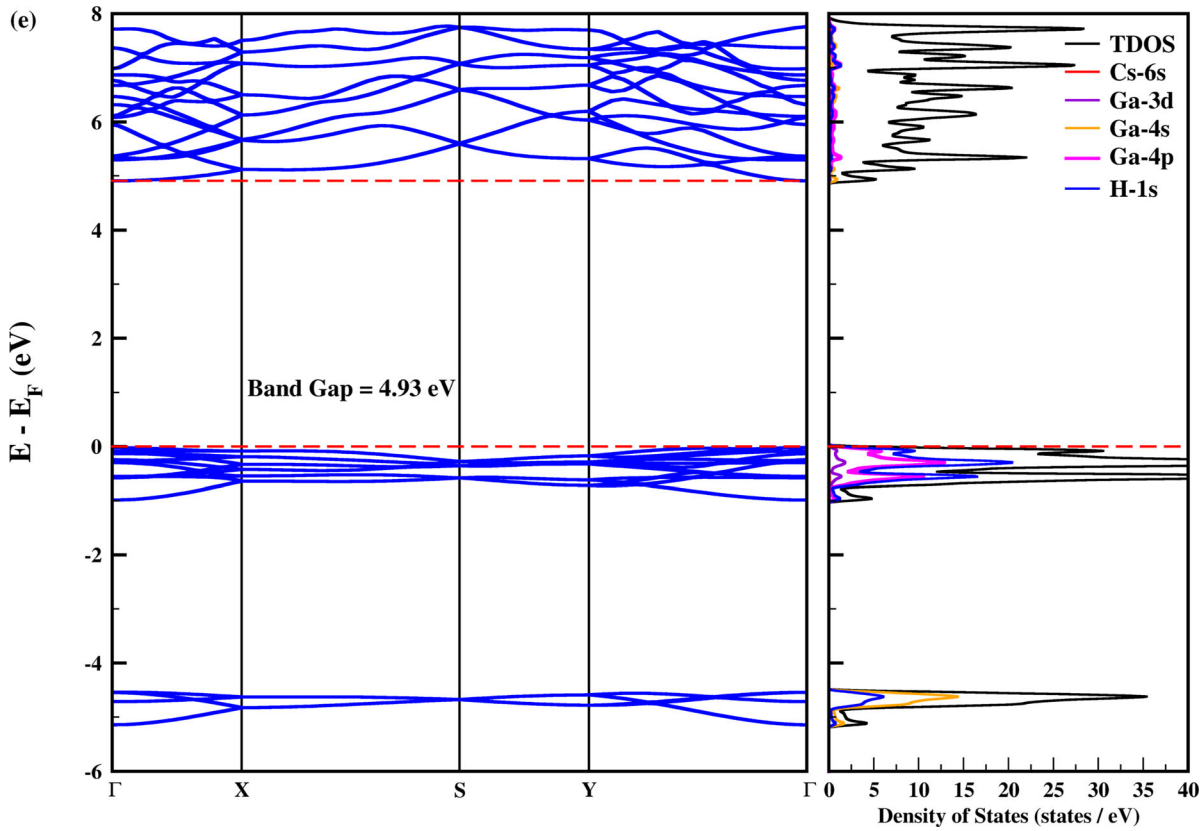

Fig. 6 continued

gaps. In addition, these results are in agreement with other studies in the literature [21, 28]. The energy distribution of electrons in the corresponding atoms and orbitals that contribute to the formation of valence and conduction bands is illustrated by the total density of states (TDOS) and partial density of states (PDOS) plots of the compounds. The Fermi level (E_F) is situated at 0 eV for the DOS plots. PDOS plots of $MGaH_4$ hydrides show a similar distribution. In the valence band near the Fermi level, it is seen that the largest contribution comes from the 1*s* orbital of H, followed by the 4*p* orbital of Ga. It is also seen that in the − 4 to − 6 eV range, the most doping comes from the 4*s* orbital of Ga. In the upper region of the Fermi level, the largest contributions in the conduction band are observed to come from the 4*s* and 4*p* orbitals of Ga and the 1*s* orbital of H.

3.5. Dynamic stability

Phonon dispersion spectra are essential for evaluating the dynamical stability of hydrides, as they provide critical insights into the vibrational behavior of the crystal lattice. By analyzing these spectra, researchers can determine whether any phonon modes exhibit imaginary frequencies, which would indicate potential structural instability. Phonon dispersion analysis also offers valuable information regarding phase transitions, the presence of soft modes that may lead to structural distortions, and the material's response to external stresses. This comprehensive vibrational data is crucial for the development of stable hydride materials with desirable properties for applications in photovoltaics, optoelectronics, and advanced technologies.

Figure 7(a)–(e) presents the phonon dispersion curves for $MGaH_4$ (M = Li, Na, K, Rb, Cs) hydrides, illustrating their evolution along the high-symmetry directions (Γ–X–S–Y–Γ) within the Brillouin zone. The crystal structure of $MGaH_4$ contains twenty-four atoms per unit cell, resulting in seventy-two phonon branches, comprising three acoustic and sixty-nine optical modes. The absence of negative phonon frequencies in the dispersion bands shown in Fig. 7 confirms the dynamical stability of these materials. Furthermore, additional evidence of stability is provided by the acoustic mode, which exhibits zero frequency at the Γ-point, in accordance with fundamental stability criteria.

3.6. Thermal properties

The Debye temperature (θ_D) in solid-state physics determines the upper limit of lattice vibration energy modes and serves as a threshold for the distribution of phonon energy.

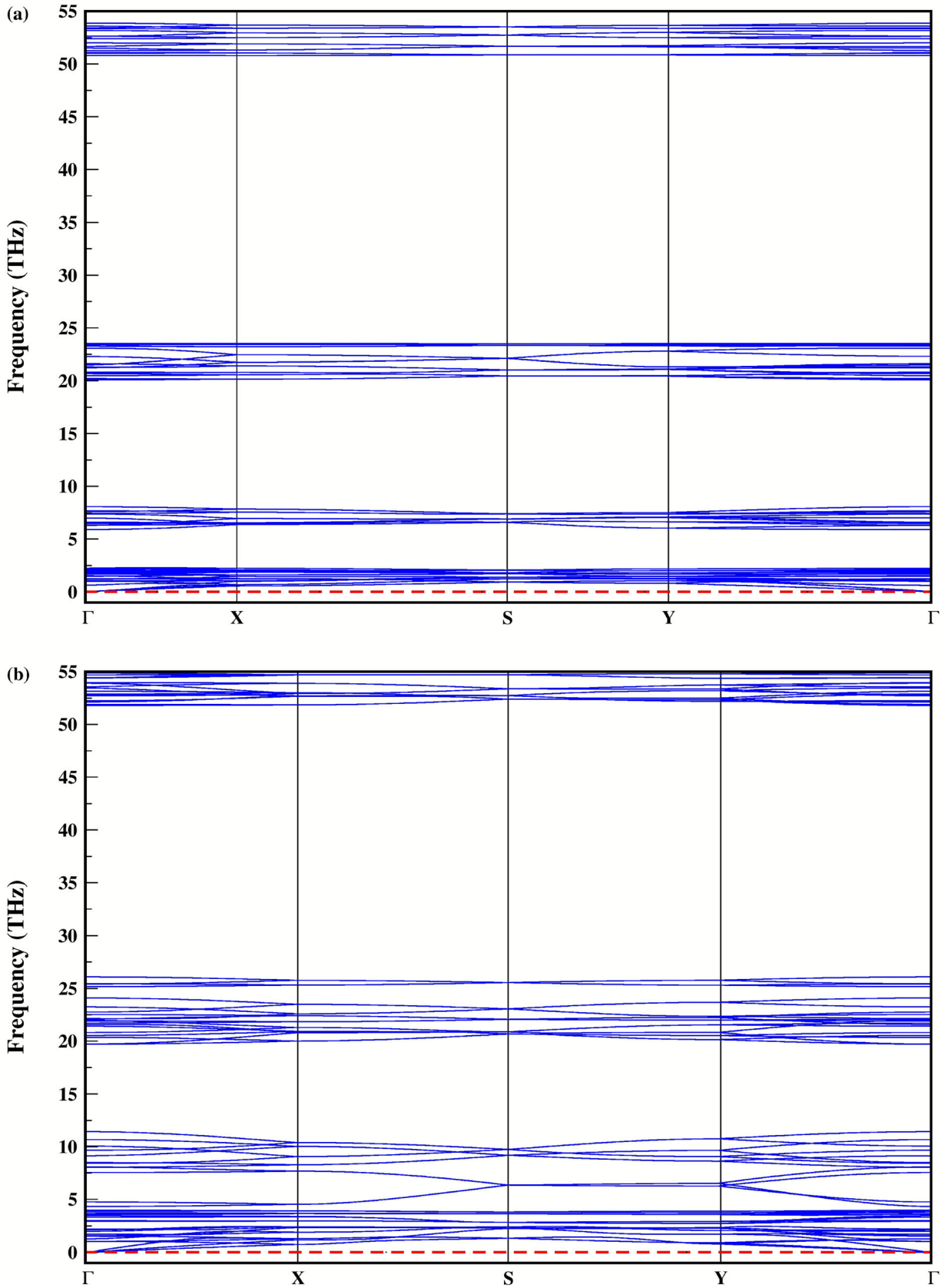

Fig. 7 The phonon dispersion curves of (**a**) $LiGaH_4$, (**b**) $NaGaH_4$, (**c**) $KGaH_4$, (**d**) $RbGaH_4$, and (**e**) $CsGaH_4$

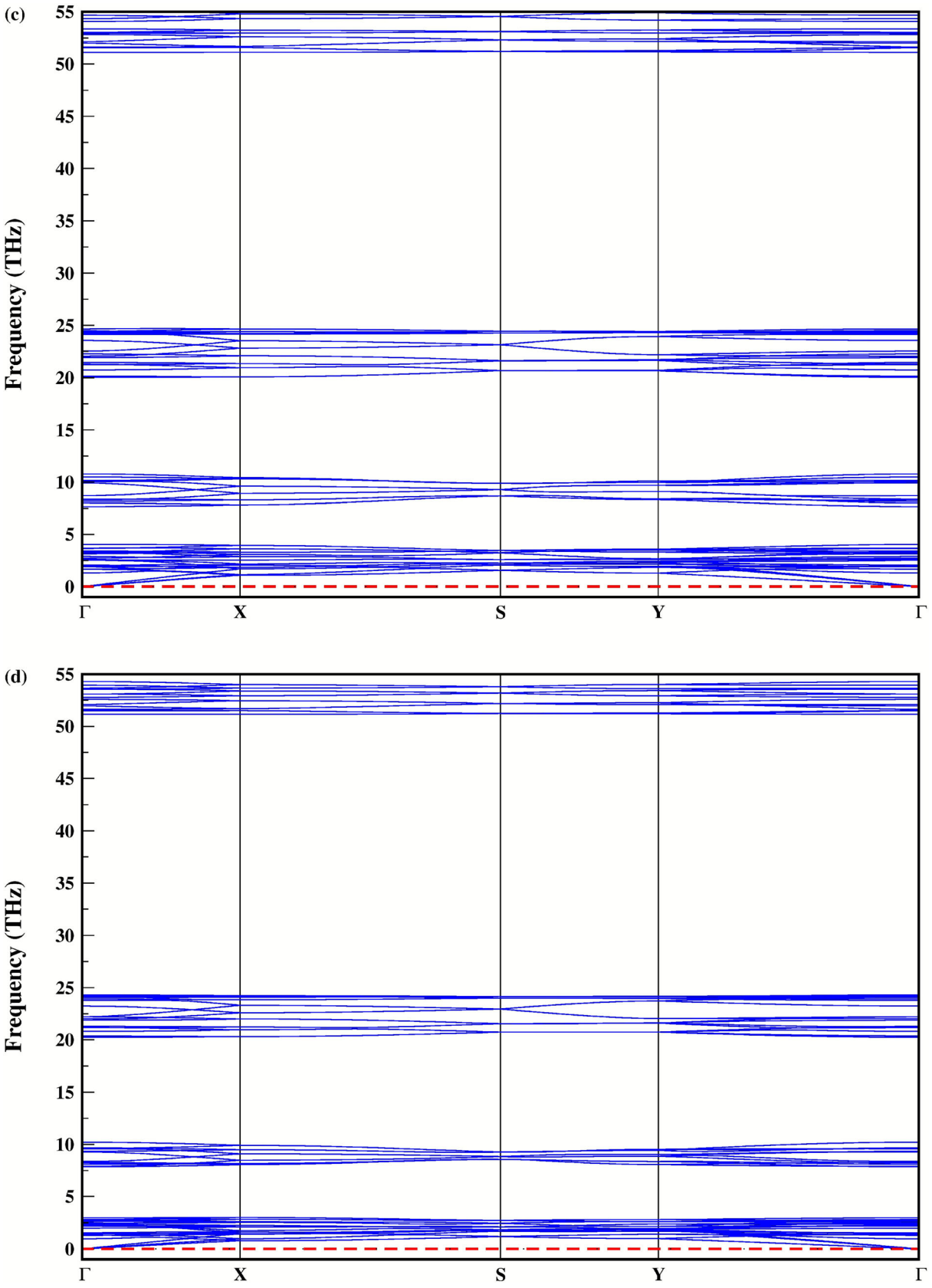

Fig. 7 continued

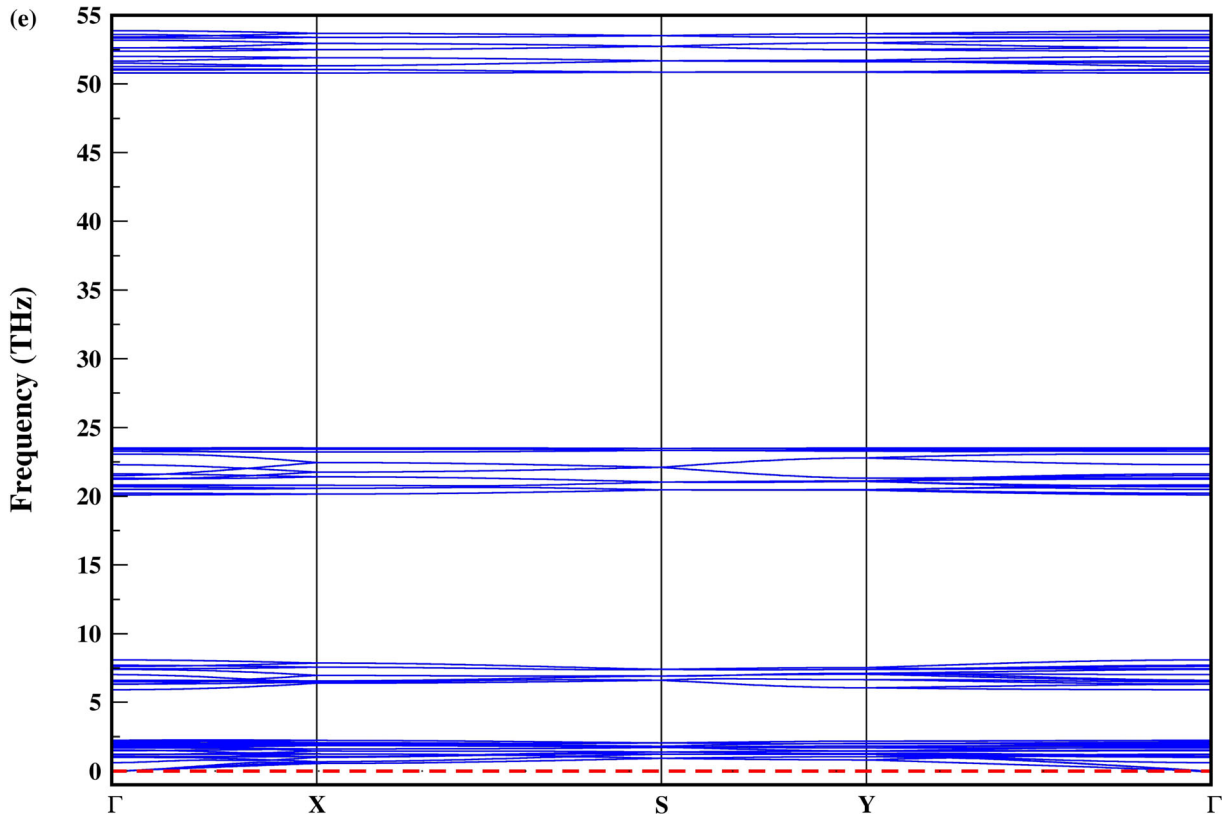

Fig. 7 continued

This parameter also provides valuable information regarding the thermal conductivity, specific heat capacity, melting temperature, lattice dynamics, and elastic constants of a material. The Anderson method [74] was implemented in this investigation to determine the θ_D. The following equation is employed to calculate θ_D using the sound velocity (v_m):

$$\theta_D = \frac{h}{k_B}\left[\left(\frac{3N}{4\pi}\right)\frac{N_A\rho}{M}\right]^{\frac{1}{3}} v_m \tag{21}$$

The equation above represents the relationship between various variables. M represents the molar mass, N represents the total number of atoms in the cell, h represents Planck's constant, ρ represents the density, N_A represents Avogadro's number, and k_B represents Boltzmann's constant. The subsequent equation can be utilized to compute the mean sound velocity (v_m).

$$v_m = \left[\frac{1}{3}\left(\frac{2}{v_t^3}+\frac{1}{v_l^3}\right)\right]^{-\frac{1}{3}} \tag{22}$$

In the present instance, "v_l" and "v_t" represent the longitudinal and transverse sound velocities, respectively. The values of v_l and v_t can be derived from:

$$v_l = \sqrt{\frac{3B+4G}{3\rho}} \tag{23}$$

$$v_t = \sqrt{\frac{G}{\rho}} \tag{24}$$

Furthermore, the acoustic Gruneisen constant γ_a is commonly employed to quantify the anharmonic properties of interactions between atoms in solids. It can be computed using the subsequent equation [75]:

$$\gamma_a = \frac{3}{2}\left(\frac{\left(3v_l^2-4v_t^2\right)}{v_l^2+2v_t^2}\right) \tag{25}$$

Table 8 presents the computed values of θ_D, the acoustic Grüneisen constant, the mass density (ρ), and the acoustic velocities (v_l, v_t, and v_a) for $MGaH_4$ compounds. $LiGaH_4$ has a Debye temperature of 352.04 K, which is higher than that of $KGaH_4$ (309.47 K), $NaGaH_4$ (245.16 K), $RbGaH_4$ (244 K), and $CsGaH_4$ (168.26 K). Thus, $LiGaH_4$ at a temperature of 352.04 K has the greatest chemical bond strength. Furthermore, the expansion coefficient of $LiGaH_4$ drops as the Debye temperature increases, leading to enhanced thermal stability and a lower coefficient of expansion.

Table 8 Computed properties of $MGaH_4$ (M = Li, Na, K, Rb, Cs): mass density (ρ, g/cm^3), longitudinal, transverse, and average sound velocities (v_l, v_t, v_m in m/s), Debye temperature (θ_D, K), melting temperature (T_m, K), minimum thermal conductivity (K_{min}, W/m·K), and Grüneisen parameter (γ_a)

Compound	ρ	v_t	v_l	v_m	T_m	θ_D	K_{min}	γ_a
$LiGaH_4$	1.95	2421.78	3824.57	2663.98	553.64	352.04	0.72	1.16
$NaGaH_4$	1.97	1768.60	3085.09	1964.68	468.11	245.16	0.48	1.53
$KGaH_4$	2.15	2294.37	3824.68	2538.17	494.63	309.47	0.59	1.36
$RbGaH_4$	2.02	1850.19	2991.53	2040.46	437.77	244.00	0.45	1.25
$CsGaH_4$	2.83	1390.86	2345.84	1540.38	428.38	168.26	0.29	1.40

A high-value Grüneisen constant indicates a significant level of anharmonicity. According to the data in Table 8, $KGaH_4$ has the highest γ_a value of 1.53, indicating that $KGaH_4$ has the most nonharmonicity.

The melting temperature, or melting point, of a material refers to the specific temperature at which it undergoes a phase transition from a solid to a liquid state under a given atmospheric pressure. Currently, the investigation of the melting temperature (T_m) of a substance is both intriguing and essential. Materials with greater melting temperatures exhibit reduced thermal expansion, higher cohesive energy, and higher bonding energy [76]. By utilizing the formula provided below, we have computed the T_m of $MGaH_4$ compounds using the optimized elastic constants [77].

$$T_m = 354 + 1.5(2C_{11} + C_{33}) \tag{26}$$

This expression is used to approximate the melting temperature of $MGaH_4$, and it is shown in Table 8. The estimated melting temperatures of $MGaH_4$ hydrides are quite low, demonstrating their soft nature. It is also noticed that the compound $LiGaH_4$ (553.64 K) has a much higher melting point compared to the $NaGaH_4$ (468.11 K), $KGaH_4$ (494.63 K), $RbGaH_4$ (437.77 K), and $CsGaH_4$ (428.38 K) hydrides. Thus, $LiGaH_4$ will have higher bonding and cohesive energy compared to $NaGaH_4$, $KGaH_4$, $RbGaH_4$, and $CsGaH_4$.

The minimum thermal conductivity offers valuable insight into the atomic dynamics of a crystal during heating or cooling. It represents the theoretical lower limit of a material's intrinsic thermal conductivity. One approach to determining this minimum value is through the following mathematical expression [78, 79].

$$K_{min} = k_B v_m \left(\frac{M}{n\rho N_A}\right)^{-\frac{2}{3}} \tag{27}$$

The calculated values for $MGaH_4$ hydrides are recorded in Table 8.

Consequently, the compound with a high Debye temperature exhibits the highest melting point and the highest level of hardness. This outcome is anticipated since a greater Debye temperature signifies a more robust interatomic bonding, resulting in an elevated melting temperature and increased mechanical strength. The Debye temperatures computed for $MGaH_4$ are often low, reflecting the inherent softness of these materials.

3.7. Hydrogen storage properties

The practical use of hydrogen as an alternative fuel faces challenges due to slow progress in developing materials with high hydrogen storage capacity. Hydrides have garnered significant interest in the scientific community because of their advantageous properties, such as high storage capacity, structural flexibility, and compatibility with fuel cell operating pressures. To evaluate the potential of $MGaH_4$ (M = Li, Na, K, Rb, Cs) hydrides for solid-state hydrogen storage, an analysis was conducted to determine their volumetric (C_v) and gravimetric ($C_{wt\%}$) storage capacities. The weight percentage of the studied hydrides was calculated using Eq. (28), where M_H represents the molecular weight of hydrogen, M_{Host} denotes the molecular weight of the host material, and H/M indicates the hydrogen-to-metal ratio.

$$C_{wt\%} = \left(\frac{\left(\frac{H}{M}\right)M_H}{M_{Host} + \left(\frac{H}{M}\right)M_H} x100\right)\% \tag{28}$$

The measured values of $C_{wt\%}$ for $MGaH_4$ (M = Li, Na, K, Rb, Cs) hydrides are shown in Table 9. The measured weight percentages of $LiGaH_4$, $NaGaH_4$, $KGaH_4$, $RbGaH_4$, and $CsGaH_4$ hydrides are 5.00%, 4.17%, 3.58%, 2.53%, and 1.95%, respectively. In addition, we have determined the C_v values for $MGaH_4$ (M = Li, Na, K, Rb, Cs) hydrides to be 92.81, 81.51, 71.74, 63.11, and 54.67 gH_2l^{-1}, respectively. In summary, our findings have indicated that the $LiGaH_4$ hydride exhibits the highest attained storage capacities, 5.00 wt% for $C_{wt\%}$ and 92.81 gH_2l^{-1} for C_v as compared to the discussed hydrides. These findings indicate that the $LiGaH_4$ compound has promising potential as a highly efficient choice for solid-state hydrogen storage. Furthermore, the $C_{wt\%}$ of $LiGaH_4$ hydride is close to the US-DOE target of 5.5 wt% for

Table 9 Calculated desorption temperature [T_{des} (K)], gravimetric [$C_{wt\%}$], and volumetric [C_v (gH_2l^{-1})] storage capacities for $MGaH_4$ (M = Li, Na, K, Rb, Cs) hydrides

Compound	T_{des}	$C_{wt\%}$	C_v
$LiGaH_4$	113.70	5.00	92.81
$NaGaH_4$	127.28	4.17	81.51
$KGaH_4$	172.37	3.58	71.74
$RbGaH_4$	176.70	2.53	63.11
$CsGaH_4$	183.01	1.95	54.67

2025, while the C_v target of $40gH_2l^{-1}$ is above all hydrides discussed.

Desorption temperature (T_{des}) is an important factor for hydrogen storage applications. T_{des} can be calculated using the following equation [80–83].

$$T_{des} = \frac{\Delta S}{\Delta H} \tag{29}$$

The production of hydrogen gas (H_2) is the main factor that determines the change in entropy during the breakdown process. According to scientific experts and published literature, the current consensus is that the change in entropy (ΔS) for H_2 is around -130.7 J/mol.K at standard temperature and pressure conditions [84]. The value of ΔH is the enthalpy of formation energy determined from Eq. (1). The desorption temperature values for $LiGaH_4$, $NaGaH_4$, $KGaH_4$, $RbGaH_4$, and $CsGaH_4$ are 113.70 K, 127.28 K, 172.37 K, 176.70 K, and 183.01 K, respectively. The desorption temperature measurements we got are below the specified range of T_{des} (233 to 333 K) set by the United States Department of Energy for the year 2025 [85, 86].

In $MGaH_4$ (M = Li, Na, K, Rb, Cs) hydrides, the hydrogen storage capacity is determined by the interplay between mechanical and electronic properties. The size and ionic character of the alkali metal cations directly influence the crystal structure's elasticity and mechanical stability, ensuring the safe storage of hydrogen. Systems with smaller ions, such as $LiGaH_4$ and $NaGaH_4$, form more compact and mechanically robust structures, whereas larger ions (K, Rb, Cs) increase lattice flexibility but also raise the risk of structural instability. From an electronic perspective, the charge distribution between the metal cations and Ga–H units optimizes hydrogen binding energies and governs the thermodynamics of adsorption–desorption. In this context, mechanical stability protects the material against volume changes during hydrogen uptake, while the electronic structure chemically stabilizes hydrogen. Consequently, in $MGaH_4$ hydrides, high and reversible hydrogen storage capacity is achieved through a balanced combination of suitable mechanical properties and favorable electronic interactions.

4. Conclusions

Using density functional theory (DFT), this study extensively investigated the structural, electronic, mechanical, dynamic, optical, thermal, and hydrogen storage properties of MGaH4 (M = Li, Na, K, Rb, Cs) compounds. The results are novel as no such comprehensive study on these compounds exists in the literature. The thermal stability of the compounds is determined by calculating the formation energy. The formation energy values obtained for all compounds are negative. Thus, it is clear that the compounds are stable. The band gaps for the calculated hydrides were obtained as 4.57 eV for $LiGaH_4$, 4.68 eV for $NaGaH_4$, 5.00 eV for $KGaH_4$, 5.00 eV for $RbGaH_4$, and 4.93 eV for $CsGaH_4$. The materials exhibit semiconducting properties with a wide band gap. The elastic constant and phonon calculations show that all compounds are mechanically and dynamically stable. Besides, according to the B/G ratio, which gives information about the hardness of the material, all compounds exhibit brittle properties. LiGaH4 has the largest gravimetric (5.00 wt%) and volumetric (92.81 gH_2l^{-1}) storage capacity among the compounds. In addition, the debye temperatures were also calculated for the compounds, and LiGaH4 (352.04 K) has the largest temperature value.

Acknowledgements This study was supported by the Kırşehir Ahi Evran University under Scientific Research Project No: TBY.A1.24.001.

Declaration of generative AI and AI-assisted technologies in the writing process During the preparation of this work, the author(s) used an artificial intelligence tool to improve the language and readability of the study. After using this tool/service, the author(s) reviewed and edited the content as needed and take(s) full responsibility for the content of the publication.

References

[1] Global Energy & CO2 Status Report 2019 – Analysis, https://www.iea.org/reports/global-energy-co2-status-report-2019
[2] S-X Mao, J-Y Song, W-S Zhu, H-M Li, J-Y Pang, D-B Dang and Y Bai *Fuel* **352** 128982 (2023)
[3] Y Dou, A Wang, L Zhao, X Yang, Q Wang, W Zhu and D Shang *Journal of Colloid and Interface Science* **650** 943 (2023)
[4] L Eicke and N De *Energy Research & Social Science* **93** 102847 (2022)
[5] A Bird's Eye view on process and engineering aspects of hydrogen storage - ScienceDirect, https://www.sciencedirect.com/science/article/pii/S136403211830248X?casa_token=ejP4mjh3e-

oAAAAA:gWtCzpo5vEhtz7RzgXaHzRcf_g2k
x6_B4FQ_eB6FF-S4652NsyNJddRe7ZcrfG_HTjZ38oyTtjk
[6] S Dutta *Journal of Industrial and Engineering Chemistry* **20** 1148 (2014)
[7] H Xia, L Zan, P Yuan, G Qu, H Dong, Y Wei, Y Yu, Z Wei, W Yan, J-S Hu, D Deng and J-N Zhang *Angewandte Chemie* **135** e202218282 (2023)
[8] B Gamisch, S Ettengruber, M Gaderer and B Dawoud, *Renewable and Sustainable Energy* (2023)
[9] I P Jain *International Journal of Hydrogen Energy* **34** 7368 (2009)
[10] P P Edwards, V L Kuznetsov, W I F David and N P Brandon *Energy Policy* **36** 4356 (2008)
[11] Novel hydrogen storage materials: A review of lightweight complex hydrides - ScienceDirect, https://www.sciencedirect.com/science/article/pii/S0925838810011436?casa_token=g60v9TRyvc8AAAAA:eKjlDtQjJf_snOmwxEdhhfq02qlGtNenXY7GVuG2WzW0LraA5nNDWkV3oGF7zlsUCKbRgEWA6Tk
[12] Frontiers | State of charge estimation of lithium-ion battery based on extended Kalman filter algorithm, https://doi.org/10.3389/fenrg.2023.1180881/full
[13] S Li, J Chen, X He, Y Zheng, C Yu and H Lu *Applied Surface Science* **623** 157036 (2023)
[14] D Chen, Y Zhu, S Han, L Anatoly, M Andrey and L Lu *Journal of Energy Storage* **60** 106587 (2023)
[15] Y Pan and J Gao *Journal of Energy Storage* **124** 116869 (2025)
[16] Y Pan and Y Zhu *Journal of Alloys and Compounds* **1021** 179661 (2025)
[17] J Gao, Y Pan, I P Jain, F Yang and J Zhu *Applied Materials Today* **44** 102755 (2025)
[18] Y Zhu, Y Pan, F Yang and J Zhu *International Journal of Hydrogen Energy* **136** 11 (2025)
[19] F Yang, Y Pan and I P Jain *International Journal of Hydrogen Energy* **140** 223 (2025)
[20] Y Pan and Y Zhu *International Journal of Hydrogen Energy* **131** 221 (2025)
[21] J F Herbst, L G Hector and W Wolf *Phys. Rev. B* **82** 024110 (2010).
[22] Ç Yamçıçıer and C Kürkçü *International Journal of Hydrogen Energy* **81** 391 (2024)
[23] P Ordejón, E Artacho and J M Soler *Phys. Rev. B* **53** R10441 (1996)
[24] J P Perdew, K Burke and M Ernzerhof *Phys. Rev. Lett.* **80** 891 (1998)
[25] N Troullier and J L Martins *Phys. Rev. B* **43** 1993 (1991)
[26] H J Monkhorst and J D Pack *Phys. Rev. B* **13** 5188 (1976)
[27] K Momma and F Izumi *J Appl Cryst* **41** 653 (2008)
[28] P Vajeeston, P Ravindran, R Vidya, H Fjellvåg and A Kjekshus *Crystal Growth & Design* **4** 471 (2004)
[29] Ç Yamçıçıer *International Journal of Hydrogen Energy* **48** 39930 (2023)
[30] S Al and Ç Yamçıçıer *Journal of Energy Storage* **91** 112033 (2024)
[31] Ç Yamçıçıer and C Kürkçü *Journal of Energy Storage* **84** 110883 (2024)
[32] G Surucu, A Gencer, A Candan, H H Gullu and M Isik *International Journal of Energy Research* **44** 2345 (2020)
[33] G Surucu, A Candan, A Gencer and M Isik *International Journal of Hydrogen Energy* **44** 30218 (2019)
[34] S Dahbi, N Tahiri, O El Bounagui and H Ez-Zahraouy *Intl J of Energy Research* **46** 8433 (2022)
[35] W Khan *Materials Science in Semiconductor Processing* **174** 108221 (2024)
[36] F Mouhat and F-X Coudert *Physical Review B* **90** 224104 (2014)
[37] L Kleinman *Physical Review* **128** 2614 (1962)
[38] M I Naher and S H Naqib *Journal of Alloys and Compounds* **829** 154509 (2020)
[39] M A Afzal and S H Naqib *Physica Scripta* **96** 045810 (2021)
[40] D Qu, C Li, L Bao, Z Kong and Y Duan *Journal of Physics and Chemistry of Solids* **138** 109253 (2020)
[41] Y Wu, Y Duan, X Wang, M Peng, L Shen and H Qi *Materials Today Communications* **33** 104651 (2022)
[42] W Voigt *Ann Arbor, Mich.]: BG Teubner [JW Edwards]* (1946)
[43] A Reuss *ZAMM - Journal of Applied Mathematics and Mechanics / Zeitschrift Für Angewandte Mathematik Und Mechanik* **9** 49 (1929)
[44] R Hill *First-principles elastic constants for the hcp transition metals Fe, Co, and Re at high pressure* p 350 (1952)
[45] A Yildirim, H Koc and E Deligoz *Chinese Physics B* **21** 037101 (2012)
[46] S F Pugh *The London, Edinburgh, and Dublin Philosophical Magazine and Journal of Science* **45** 823 (1954)
[47] Ç Yamçıçıer *Indian J Phys* (2022)
[48] A Gencer, G Surucu and S Al *International Journal of Hydrogen Energy* **44** 11930 (2019)
[49] A Savin, H Flad, J Flad, H Preuss and H G von Schnering *Angewandte Chemie* **104** 185 (1992)
[50] H Fu, D Li, F Peng, T Gao and X Cheng *Computational Materials Science* **44** 774 (2008)
[51] P Barua, M Hossain, M Ali, M Uddin, S Naqib and A Islam *Journal of Alloys and Compounds* **770** 523 (2019)
[52] X-Q Chen, H Niu, D Li and Y Li *Intermetallics* **19** 1275 (2011)
[53] R Islam, M M Hossain, M A Ali, M M Uddin and S H Naqib *RSC Advances* **12** 32994 (2022)
[54] N Miao, B Sa, J Zhou and Z Sun *Computational Materials Science* **50** 1559 (2011)
[55] Y Tian, B Xu and Z Zhao *International Journal of Refractory Metals and Hard Materials* **33** 93 (2012)
[56] D M Teter *MRS Bulletin* **23** 22 (1998)
[57] E Mazhnik and A R Oganov *Journal of Applied Physics* **126** 125109 (2019)
[58] X Gao, Y Jiang, R Zhou and J Feng *Journal of Alloys and Compounds* **587** 819 (2014)
[59] P Ravindran, L Fast, P A Korzhavyi, B Johansson, J Wills and O Eriksson *Journal of Applied Physics* **84** 4891 (1998)
[60] C M Kube *AIP Advances* **6** 095209 (2016)
[61] S I Ranganathan and M Ostoja-Starzewski *Physical Review Letters* **101** 055504 (2008)
[62] F Vahldiek *Anisotropy in single-crystal refractory compounds* (Springer) (2013)
[63] D H Chung and W R Buessem *Journal of Applied Physics* **38** 2010 (1967)
[64] V Arsigny, P Fillard, X Pennec and N Ayache *Fast and Simple Calculus on Tensors in the Log-Euclidean Framework* (eds.) J S Duncan and G Gerig, (Berlin, Heidelberg: Springer) p 115 (2005)
[65] C M Kube *Journal of Applied Physics* **120** 165105 (2016)
[66] J Wang, Y Zhou, T Liao and Z Lin *Applied Physics Letters* **89** 021917 (2006)
[67] Z Ran, C Zou, Z Wei and H Wang *Computer Physics Communications* **283** 108540 (2023)
[68] M I Naher, M A Afzal and S H Naqib *Results in Physics* **28** 104612 (2021)
[69] H Wang, Y Chen, Y Kaneta and S Iwata *Journal of Alloys and Compounds* **491** 550 (2010)
[70] H Belhadj, M Ameri, B Abbar, N Moulay, A Z Bouyakoub, O Arbouche, D Bensaid, I Ameri, S Mesbah and Y Al-Douri *Chinese Journal of Physics* **55** 1032 (2017)
[71] T-Y Tang and Y-L Tang *Chemical Physics* **570** 111897 (2023)
[72] Y C Cheng, X L Wu, J Zhu, L L Xu, S H Li and P K Chu *Journal of Applied Physics* **103** (2008)

[73] J Sun, H-T Wang, J He and Y Tian *Phys. Rev. B* **71** 125132 (2005)
[74] O L Anderson *Journal of Physics and Chemistry of Solids* **24** 909 (1963)
[75] F Arab, F A Sahraoui, K Haddadi, A Bouhemadou and L Louail *Phase Transitions* **89** 480 (2016)
[76] M I Naher and S H Naqib *Scientific Reports* **11** 5592 (2021)
[77] M E Fine, L D Brown and H L Marcus *Scripta Metallurgica* **18** 951 (1984)
[78] D S Clarke *Communicative Intent and Conventionality* (Springer) p 67 (2003)
[79] M M Hossain, M A Hossain, S A Moon, M A Ali, M M Uddin, S H Naqib, A Islam, M Nagao, S Watauchi and I Tanaka *Journal of Materials Science: Materials in Electronics* **32** 3878 (2021)
[80] R Song, Y Chen, S Chen, N Xu and W Zhang *International Journal of Hydrogen Energy* **57** 949 (2024)
[81] M Ali, Z Bibi, M W Younis, K Majeed, U Afzal, S Khan, N H Alotaibi and M Mubashir *International Journal of Hydrogen Energy* **70** 579 (2024)
[82] C Kurkcu, S Al and C Yamcicier *Eur. Phys. J. B* **95** 180 (2022)
[83] S Al, C Kurkcu and C Yamcicier *International Journal of Hydrogen Energy* **45** 4720 (2020)
[84] Q Zeng, K Su, L Zhang, Y Xu, L Cheng and X Yan *Journal of Physical and Chemical Reference Data* **35** 1385 (2006)
[85] J Lyu, R Elman, L Svyatkin and V Kudiiarov *Journal of Alloys and Compounds* **938** 168618 (2023)
[86] M Mubashir, M Ali, Z Bibi, M W Younis and M Muzamil *International Journal of Hydrogen Energy* **50** 774 (2024)